© 2018. Published by The Company of Biologists Ltd | Journal of Cell Science (2018) 131, jcs217620. doi:10.1242/jcs.217620

RESEARCH ARTICLE

New ubiquitin-dependent mechanisms regulating the Aurora B–protein phosphatase 1 balance in *Saccharomyces cerevisiae*

Rini Ravindran[1], Paula Polk[2], Lucy C. Robinson[1] and Kelly Tatchell[1,*]

ABSTRACT

Protein ubiquitylation regulates many cellular processes, including cell division. We report here a novel mutation altering the *Saccharomyces cerevisiae* E1 ubiquitin-activating enzyme (*uba1-W928R*) that suppresses the temperature sensitivity and chromosome loss phenotype of a well-characterized Aurora B mutant (*ip1-2*). The *uba1-W928R* mutation increases histone H3-S10 phosphorylation in the *ipl1-2* strain, indicating that *uba1-W928R* acts by increasing Ipl1 activity and/or reducing the opposing protein phosphatase 1 (PP1; Glc7 in *S. cerevisiae*) phosphatase activity. Consistent with this hypothesis, Ipl1 protein levels and stability are elevated in the *uba1-W928R* mutant, likely mediated via the E2 enzymes Ubc4 and Cdc34. In contrast, the *uba1-W928R* mutation does not affect Glc7 stability, but exhibits synthetic lethality with several *glc7* mutations. Moreover, *uba1-W928R* cells have an altered subcellular distribution of Glc7 and form nuclear Glc7 foci. These effects are likely mediated via the E2 enzymes Rad6 and Cdc34. Our new *UBA1* allele reveals new roles for ubiquitylation in regulating the Ipl1–Glc7 balance in budding yeast. While ubiquitylation likely regulates Ipl1 protein stability via the canonical proteasomal degradation pathway, a non-canonical ubiquitin-dependent pathway maintains normal Glc7 localization and activity.

This article has an associated First Person interview with the first author of the paper.

KEY WORDS: Uba1, Aurora B, PP1, Protein stability, Protein localization, E2 ubiquitin-conjugating enzymes, Chromosome segregation

INTRODUCTION

Protein ubiquitylation is a common and complex protein modification in which the highly conserved ubiquitin protein is covalently linked to the ε amino group of lysine residues. Most of these modification events regulate protein stability and quality control via the proteasome or through autophagy, but ubiquitylation can result in a variety of other outcomes, including changes to subcellular localization, protein–protein interactions or enzymatic activity (reviewed in Rape, 2018). The major substrate for ubiquitylation is ubiquitin itself, in which seven conserved lysine residues and the N-terminal methionine residue can serve as substrates for additional rounds of ubiquitylation, leading to polyubiquitylated proteins. Different linkages in polyubiquitin can adopt unique structures, leading to different fates for a protein (Komander and Rape, 2012). Specificity is dictated by a diverse array of proteins containing ubiquitin-binding domains (UBDs), which bind to specific sets of ubiquitylated proteins. Ubiquitin-binding proteins associated with the proteasome escort mostly K48- and K11-linked polyubiquitin to the proteasome (Chau et al., 1989; Jin et al., 2008) or to the Cdc48–Ufd1–Npl4 segregase (Ye et al., 2003), whereas proteins with affinity for monoubiquitin or polyubiquitin formed with other linkages regulate ubiquitylated proteins in other ways (Komander and Rape, 2012). Finally, the attachment of ubiquitin can be reversed by de-ubiquitylating enzymes (DUBs), which make this modification highly dynamic (Mevissen and Komander, 2017).

Protein ubiquitylation is carried out by the ordered activities of the E1 ubiquitin-activating enzyme, which transfers ubiquitin to an E2 ubiquitin-conjugating enzyme (Lorenz et al., 2013). Ubiquitin is then transferred to the substrate lysine residue, usually with the assistance of an E3 ubiquitin ligase. There is a clear hierarchy in the abundance and conservation of these enzyme classes. One or a few highly conserved E1 enzymes activate ∼10 to ∼70 E2s, depending on the species (Jue et al., 2015). E3s number in the hundreds (Finley et al., 2012). Given this hierarchy, interest in specific ubiquitin-dependent processes has logically focused on E2 and E3 enzymes. However, the structures of several E1–E2 complexes indicate that different E2s associate with unique structural elements of the E1 (Olsen and Lima, 2013; Lv et al., 2017), suggesting a potential regulatory role for the E1 enzyme. In addition, Uba1, the sole E1 enzyme in *Saccharomyces cerevisiae*, is post-translationally modified by phosphorylation, ubiquitylation and succinylation at multiple sites (Albuquerque et al., 2008; Holt et al., 2009; Swaney et al., 2013; Fang et al., 2014), providing potential mechanisms for regulating specific interactions with E2 enzymes.

Whether or not E1 contributes to selectivity, the effects of impaired E1 activity in model systems have demonstrated the wide array of processes regulated by ubiquitylation. Study of loss-of-function mutations in *Drosophila melanogaster UBA1* have shown that mutations in this E1 reduce fly lifespan and impair motor function (Liu and Pfleger, 2013). Characterization of a *Caenorhabditis elegans uba1-1* mutant revealed roles for ubiquitylation in regulating sperm fertility, control of body size and sex-specific development (Kulkarni and Smith, 2008). In *S. cerevisiae*, the temperature-sensitive *uba1-204* allele has been used to show that ubiquitin conjugates are necessary for targeting the ubiquitin-binding adaptor protein Rad23 to the proteasome (Ghaboosi and Deshaies, 2007). Similarly, mammalian cell lines that harbor mutations in the E1 gene or in other genes that affect E1 function have demonstrated important roles for ubiquitylation in the heat-shock response and in regulation of cell cycle progression (Kulka et al., 1988; Salvat et al., 2000; Lao et al., 2012; Sugaya et al., 2014).

Some mutations in E1 confer thermosensitivity and lead to cell cycle arrest, which provided early evidence that ubiquitylation is

[1]Department of Biochemistry and Molecular Biology, Louisiana State University Health Sciences Center, Shreveport, LA 71130, USA. [2]Research Core Facility Genomics Core, Louisiana State University Health Sciences Center, Shreveport, LA 71130, USA.

*Author for correspondence (ktatch@lsuhsc.edu)

R.R., 0000-0002-2581-5164; P.P., 0000-0002-0018-233X; L.C.R., 0000-0001-6454-040X; K.T., 0000-0002-5330-410X

Received 9 March 2018; Accepted 11 July 2018

Journal of Cell Science (2018) 131, jcs217620. doi:10.1242/jcs.217620

required for cell cycle progression through both S and G2 phases (Finley et al., 1984; Ayusawa et al., 1992; Nishitani et al., 1992). The anaphase-promoting complex (APC/C) and Skp1–Cdc53–F-box (SCF) E3 ligases are responsible for targeting cell cycle-specific substrates to the proteasome (reviewed in Wickliffe et al., 2009). However, several lines of evidence also show that ubiquitylation regulates proteasome-independent cell cycle events. For example, in human cells, ubiquitylation of components of the chromosome passenger complex (CPC) trigger CPC binding to centromeres during prometaphase (Vong et al., 2005). The CPC is a four subunit protein complex, composed of Aurora B kinase (Ipl1 in *S. cerevisiae*) and three auxiliary subunits (Carmena et al., 2012). Prior to anaphase, Aurora B/Ipl1 phosphorylates kinetochore proteins, which destabilizes their attachment to spindle microtubules, and allows correction of improper kinetochore–microtubule interactions (reviewed in Tanaka et al., 2005). Thus, Aurora B activity creates unattached kinetochores and activates the spindle assembly checkpoint (SAC), which monitors bipolar chromosome attachment to the mitotic spindle and delays anaphase until proper bi-orientation is achieved (Pinsky et al., 2006b). In fission yeast and human cells, Aurora B is localized to the inner centromere prior to anaphase via its CPC partner proteins, and this localization is controlled by histone H3 and H2A phosphorylation (Kelly et al., 2010; Yamagishi et al., 2010). In human cells, a cullin-based ubiquitin ligase (Cul3) interacts with three different substrate-specific adaptor proteins to ubiquitylate Aurora B and target it differently to the spindle midzone and midzone microtubules (Sumara et al., 2007; Maerki et al., 2009). Ubiquitylated Aurora B is subsequently removed from chromosomes by the AAA+ ATPase Cdc48 (known as p97 and VCP in mammals) and its adaptor proteins Ufd1-Npl4, which facilitates nuclear reformation at the end of mitosis (Ramadan et al., 2007). Following anaphase, Aurora B migrates from chromosomes to the central spindle where it plays a role in cytokinesis (Carmena et al., 2012).

The protein phosphatase PP1 (Glc7 in *S. cerevisiae*) opposes the CPC activity, dephosphorylating kinetochore proteins to stabilize kinetochore–microtubule interactions and silence the SAC (Pinsky et al., 2009; Vanoosthuyse and Hardwick, 2009; Liu et al., 2010; Wurzenberger et al., 2012). Therefore, Aurora B and PP1 activities must be tightly balanced to ensure fidelity of mitotic chromosome segregation. In addition to opposing Aurora B at kinetochores, PP1 has many additional regulatory roles, ranging from carbohydrate metabolism to learning and memory (reviewed in Virshup and Shenolikar, 2009; Bollen et al., 2010). The activity of the highly conserved PP1 catalytic subunit is tightly controlled by a large collection of binding proteins that associate with PP1 via short conserved motifs, the most well studied of which is the RVxF motif found in many PP1-binding proteins (Bollen et al., 2010). Outside these motifs, most PP1-binding proteins are not highly conserved but allow PP1 to serve as the catalytic subunit for a large number of tissue- and cell type-specific phosphatase holoenzymes. Remarkably, Sds22 and Ypi1 (also known as inhibitor 3 or PPP1R11 in mammals), two of the most highly conserved PP1-binding partners, have been implicated in regulating the PP1 phosphatase activity that opposes Aurora B (Hisamoto et al., 1995; Peggie et al., 2002; Bharucha et al., 2008; Posch et al., 2010; Wurzenberger et al., 2012; Eiteneuer et al., 2014). Genetic studies have also identified the AAA+ ATPase Cdc48 and its adaptor Shp1 (known as p47 or NSFL1C in humans) (Zhang et al., 1995; Cheng and Chen, 2010; Böhm, 2011; Robinson et al., 2012; Cheng and Chen, 2015) as Glc7 regulators. Mutations in any of these regulatory proteins lead to mitotic delay or arrest, reduce Glc7 nuclear localization and cause formation of Glc7 aggregates (Peggie et al., 2002; Bharucha et al., 2008; Cheng and Chen, 2010, 2015). The observation that Glc7 aggregate formation is blocked by cycloheximide in *cdc48* and *shp1* mutants led Cheng and Chen (Cheng and Chen, 2015) to propose that these regulators participate in the folding or maturation of nascent Glc7.

Genetic studies using conditional *IPL1* mutant alleles have been instrumental in identifying factors that regulate Ipl1, Glc7 and the kinetochore (Tung et al., 1995; Cheeseman et al., 2002; Peggie et al., 2002; Zhang et al., 2005; Pinsky et al., 2006a; Bharucha et al., 2008; Ng et al., 2009; Cheng and Chen, 2010; Tatchell et al., 2011; Robinson et al., 2012; Makrantoni et al., 2017). Surprisingly, considering the importance of ubiquitylation in cell cycle progression, relatively few *IPL1* suppressors or enhancers alter direct components of ubiquitylation pathways. Mutations altering the ubiquitin-conjugating enzyme Rad6 and its E3 partner Bre1 weakly suppress the temperature sensitivity of *ipl1-2* mutants indirectly, through Set1-dependent methylation of kinetochore protein Dam1 (see Latham et al., 2011 and below). A deletion mutation of the E3 SLX5 has the opposite effect, causing *ipl1-321* mutants to grow more slowly (Ng et al., 2009). We report here that a missense mutation in the E1 ubiquitin activating enzyme *UBA1* suppresses *ipl1-2*. Characterization of this *UBA1* allele reveals novel roles for ubiquitylation in Ipl1 and Glc7 regulation.

RESULTS

A mutation in *UBA1* suppresses the temperature sensitivity and chromosome loss of *ipl1-2*

A previously uncharacterized *ipl1-2* suppressor mutation, denoted *revertant 100* (*rev100*), segregates as a single Mendelian allele for which slow growth co-segregates with suppression of *ipl1-2*. *rev100* suppresses the temperature sensitivity of *ipl1-2* up to 33°C (Fig. 1A). In an *IPL1* WT background, *rev100* confers slow growth at 24°C, sensitivity to low (14°C) and high (37°C) temperatures and sensitivity to caffeine (Fig. 1B). *rev100* causes slight sensitivity to 0.1 M CsCl in growth medium but higher resistance to 0.1 M LiCl in growth medium (Fig. 1B). To identify the mutation responsible for *ipl1-2* suppression, whole-genome sequence analysis was performed on pooled DNA from six backcrossed *rev100* ascoporal clones. A total of 62 differences between the *rev100* mutant DNA and our parent strain (KT1113) were found. Of these, 18 were observed in all sequence reads (Table S1). Given the range of physiological pathways impacted by ubiquitin, a likely candidate for the *rev100* mutation is the non-synonymous T to C transversion in *UBA1*, which results in a tryptophan to arginine missense mutation at residue 928 in Uba1, the essential ubiquitin-activating E1 enzyme. We confirmed that the T to C transversion is present in a *rev100* mutant strain by Sanger sequence analysis of PCR-amplified *UBA1* DNA. A cross between a *rev100* strain (KT3300) and a *trp3::KanMX* deletion strain (EG2365-1C) gave a map distance of 2.4 map units (41P:2T:0NPD). This tight linkage would be predicted if the *rev100* mutation lies in *UBA1*, which is adjacent to the *TRP3* locus. Finally, we transformed an *ipl1-2 rev100* strain with a replicating yeast shuttle vector containing *UBA1*. The *UBA1*-containing plasmid restored the temperature sensitivity and complemented the growth defects caused by *rev100* (Fig. 1C). Taken together, these results indicate that *rev100* is a new allele of *UBA1*. Henceforth, we refer to the suppressor mutation in *rev100* as *uba1-W928R*.

A key role of Ipl1 is to ensure correct bipolar attachment of chromosomes to spindle microtubules by phosphorylating kinetochore proteins, which destabilizes attached microtubules. Loss of Ipl1 activity results in increased rates of chromosome loss and cell death (Chan and Botstein, 1993; Biggins et al., 1999). To determine whether

Journal of Cell Science (2018) 131, jcs217620. doi:10.1242/jcs.217620

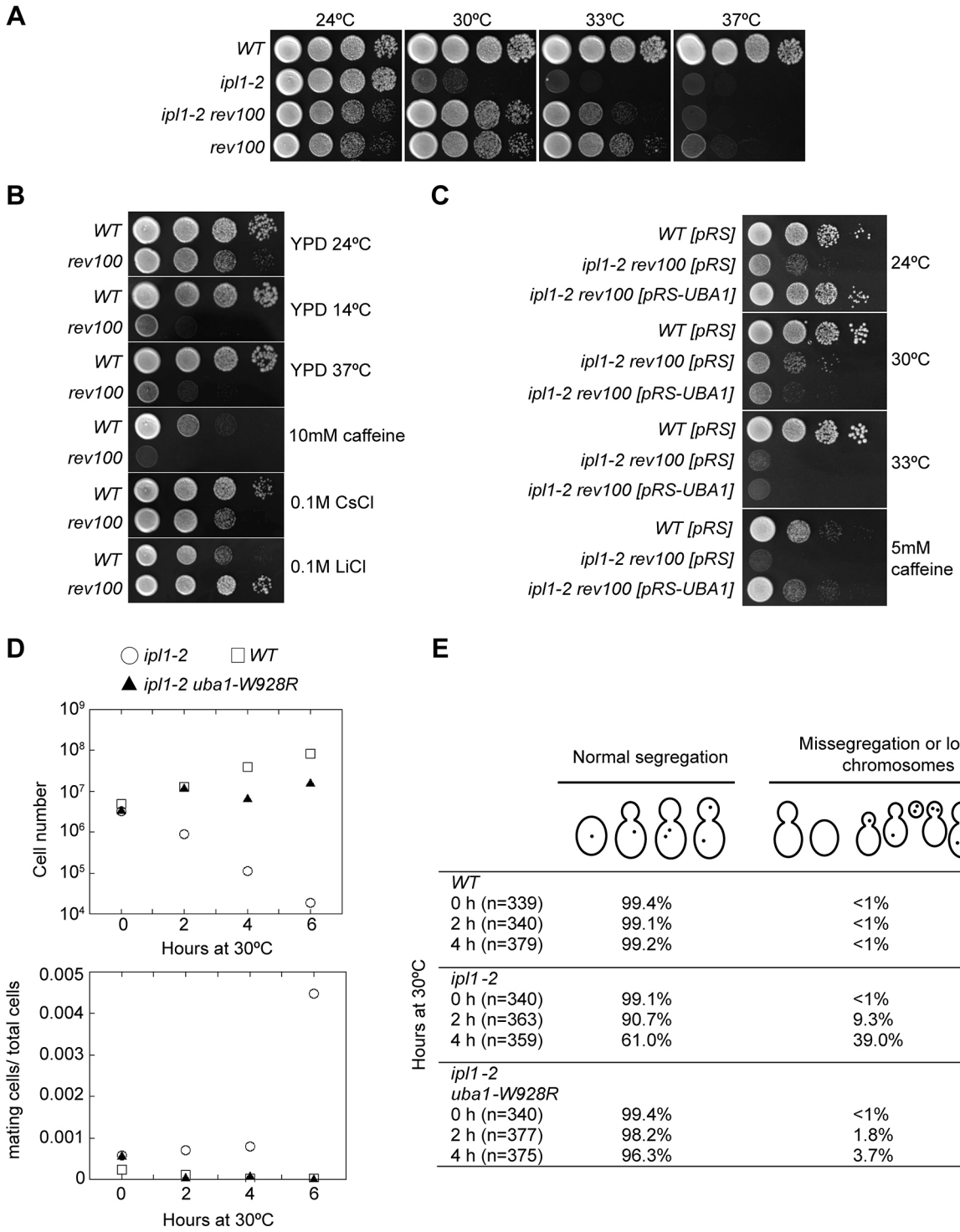

Fig. 1. A missense mutation in *UBA1*, *uba1-W928R*, suppresses the temperature sensitivity of *ipl1-2*. (A–C) Cultures of the designated genotypes were serially diluted onto media and imaged after incubation for 40–44 h at 24°C unless designated otherwise. (A) Serial dilutions of *WT* (KT1113), *ipl1-2* (KT1829), *ipl1-2 rev100* (*uba1-W928R*) (KT3476), and *rev100* (KT3474). (B) Serial dilutions of *WT* (KT1113) and *rev100* (KT3300). (C) Serial dilutions of *WT* (KT1113) and *ipl1-2 rev100* (KT3476) strains transformed with either the empty vector (pRS316) or the vector containing *UBA1* (pRS316-*UBA1*). (D) *WT* (KT1113×KT1963), *ipl1-2* (KT1963×KT1829), and *ipl1-2 uba1-W928R* (KT1963×KT3474) diploid strains were grown to log phase in YPD medium at 24°C, shifted to 30°C for the designated times, and assayed for cell viability (upper panel) and mating ability (lower panel) at each time point. (E) Segregation of GFP-tagged chromosome IV was analyzed in *WT* (KT3992), *ipl1-2* (KT3993) and *ipl1-2 uba1-W928R* (KT3995) cells incubated at 30°C for 2 h and 4 h.

uba1-W928R suppresses chromosome loss in the *ipl1-2* mutant, we monitored rates of chromosome III loss in diploid strains homozygous for both *ipl1-2* and *uba1-W928R*. Diploid yeast strains monosomic for chromosome III are able to mate. Therefore, acquisition of mating ability by diploid strains can be used as a read-out for chromosome III loss. Diploid yeast strains were grown at 24°C to mid-log phase and shifted to 30°C. Cell viability and mating ability were assayed after the temperature shift. As expected, the homozygous *ipl1-2* diploid with

Journal of Cell Science (2018) 131, jcs217620. doi:10.1242/jcs.217620

WT UBA1 showed loss of cell viability and an increase in the mating ability at 30°C (open circles in Fig. 1D). In contrast, the viability and mating ability of the homozygous *uba1-W928R ipl1-2* strain did not change following the temperature shift (filled triangles in Fig. 1D). We also monitored the loss of *lacO*-tagged chromosome IV in strains expressing a GFP-tagged lac repressor (Straight et al., 1997). In *ipl1-2* mutant cells, 39% of cells grown at 30°C for 4 h either had an abnormal segregation pattern of the *lacO* array or no fluorescence. Loss of fluorescence can occur upon the loss of chromosome XV, which bears the GFP–lacI gene. The missegregation frequency was reduced to 3.7% in the *ipl1-2 uba1-W928R* strain (Fig. 1E). Taken together, these results indicate that *uba1-W928R* rescues viability and suppresses chromosome loss due to *ipl1-2*.

The W928R change in Uba1 is predicted to alter the conformation between the main body of Uba1 and its E2-binding domain

Uba1 transfers an activated ubiquitin to an E2-conjugating enzyme, which binds Uba1 via the ubiquitin fold domain (UFD). The UFD undergoes distinct movement during the E1–E2 handoff, made possible by a flexible β-hairpin linker between the UFD and the main body of Uba1 (Lee and Schindelin, 2008; Olsen and Lima, 2013). W928, which is conserved in all E1 proteins (Fig. 2A), is located adjacent to the β-hairpin linker (residues 915 to 927), tethering the main body of the E1 enzyme to the UFD (Fig. 2B). Interestingly, studies in *S. pombe* that compared Uba1 structures with and without the E2 substrate show that UFD rotation is achieved by bending that begins immediately after W928, with a complementary twisting of the β-hairpin to maintain interactions between the Uba1 core (adenylation domain) and the UFD linker (Olsen and Lima, 2013). These specific contacts permit attainment of the correct UFD conformation to facilitate E2 enzyme recruitment. We reasoned that a tryptophan to arginine mutation at this critical residue could alter conformational changes needed for binding of some E2 enzyme substrates. To investigate possible structural consequences of the tryptophan to arginine mutation *in silico*, we modeled the change with PyMOL using the published *S. cerevisiae* Uba1 structure (PDB: 3CMM) (Fig. 2C). Replacing the W928 residue (red) with a positively charged arginine residue breaks hydrogen bonding with T583. Also, R928 is aligned away from the hydrophobic pocket (purple), further increasing repulsive forces from the adjacent R581 (green) (Fig. 2C, right panel), which may distort the rotation of the UFD core. Thus, the *uba1-W928R* mutation is likely to disrupt the conformation between the UFD and the main body of Uba1, and could alter the overall level of protein ubiquitylation, as has been reported previously for the *uba1-204* allele (Ghaboosi and Deshaies, 2007). To test this possibility, we grew wild-type (*WT*), *uba1-W928R* and *uba1-204* strains at 24°C to mid-log phase, raised the temperature to 37°C, and monitored protein ubiquitylation by immunoblot analysis. As previously reported (Ghaboosi and Deshaies, 2007), protein ubiquitylation drops rapidly in the *uba1-204* strain after the temperature shift (Fig. 2D). In contrast, protein-conjugated ubiquitin levels are reduced in the *uba1-W928R* strain but remain constant at all temperatures. Furthermore, the increased level of protein ubiquitylation that was observed for the *WT* strain after an 1 h incubation at 37°C was not recapitulated in the *uba1-W928R* strain. The *uba1-204* allele does not suppress *ipl1-2* (Fig. S1), likely because *uba1-204* strains retain Uba1 function at 30°C, the non-permissive temperature for *ipl1-2* cells.

uba1-W928R mutants exhibit reduced protein turnover

To address the extent to which the ubiquitylation defect of *uba1-W928R* impacts protein turnover, we tested for a possible defect in N-end rule proteasomal degradation (Varshavsky, 1996) by using a copper-inducible *URA3* reporter gene coupled to an N-end degron (Varshavsky, 2005; Hanna et al., 2006). The rate of growth of strains expressing this reporter in the absence of uracil and presence of copper inversely reflects the rate of degradation of the Ura3 reporter protein. A *rad6*Δ strain was used as a positive control, since the requirement for Rad6 as the E2 enzyme for the N-end rule pathway is well established (Dohmen et al., 1991). As expected, we observed that a *rad6*Δ mutant displays a strong growth advantage over *WT* when cultured on medium lacking uracil. The *uba1-W928R* strain grows better than *WT* but not as well as *rad6*Δ cells (Fig. 2E). To confirm that the turnover of the Ura3 reporter protein is reduced in the *uba1-W928R* strain, we performed cycloheximide-chase analyses. We observed rapid degradation of the Ura3 reporter protein in the *WT* strain, with a half-life of ∼10 min. In contrast, the *uba1-W928R* mutant shows stabilization of the Ura3 reporter protein accompanied by an increased steady-state level (Fig. 2F). The *rad6*Δ mutant exhibits very high levels of Ura3. Thus, *uba1-W928R* causes a partial defect in proteasomal degradation via the N-end rule pathway. Since Rad6 is the downstream E2 enzyme largely responsible for N-end-rule-mediated protein degradation, this result also suggests that the *uba1-W928R* mutation impairs Rad6-dependent ubiquitylation.

Rad6 also has a well-characterized role in post-replicative DNA repair (Cejka et al., 2001; Giannattasio et al., 2005). To test the possibility that *uba1-W928R* causes a defect in DNA repair, we assayed the sensitivity of *WT* and *uba1-W928R* strains to UV irradiation. A *rad9*Δ strain, defective in the DNA damage-induced cell cycle checkpoint (Weinert and Hartwell, 1988, 1990), was used as the positive control. We observed that *uba1-W928R* mutant strains are more sensitive to UV radiation than *WT* cells (Fig. 2G). The *uba1-W928R rad9*Δ double mutant is more sensitive than either of the single mutants (Fig. 2G; Fig. S2), indicating that *uba1-W928R* cells are defective in DNA repair. These results provide further evidence that *uba1-W928R* reduces ubiquitylation mediated by Rad6.

uba1-W928R mutants exhibit a mitotic cell cycle delay

uba1-W928R cells are larger (Fig. 3D) and slower growing (Fig. 1A) than *WT* cells. To determine whether *uba1-W928R* mutant cells are delayed in mitotic progression, we synchronized cells in G1 using α-factor, released them into fresh medium and assayed levels of Pds1 (securin), which accumulates in mitosis and is rapidly degraded at the onset of anaphase. The strains also contain GFP–Spc42, a component of the spindle pole body, allowing direct monitoring of spindle length. As shown in the top panel of Fig. 3A, Pds1 rapidly accumulates after release from the α-factor block in WT cells and is largely degraded before 90 min, indicating that most of the cells have entered anaphase by 90 min. In contrast, *uba1-W928R* cells are delayed in mitosis for an additional 30–60 min. We also measured the distance between the two spindle pole bodies in these cells and confirmed that formation of long spindles correlates with Pds1 degradation. At 120 mins after release from α-factor, 60% of the *uba1-W928R* mutant cells have long spindles (defined by distance between the spindle pole bodies greater than 2.5 µm) as compared to 20% for the *WT* (Fig. 3B). Thus, *uba1-W928R* cells exhibit a delay in anaphase entry. Such a delay could result from a failure to terminate the spindle assembly checkpoint (SAC). To test whether SAC activation is responsible for the mitotic delay observed for *uba1-W928R* cells, we compared Pds1 kinetics in *mad1*Δ *uba1-W928R* cells and *uba1-W928R* single-mutant cells. The kinetics of Pds1 appearance and disappearance are identical in *uba1-W928R*

Journal of Cell Science (2018) 131, jcs217620. doi:10.1242/jcs.217620

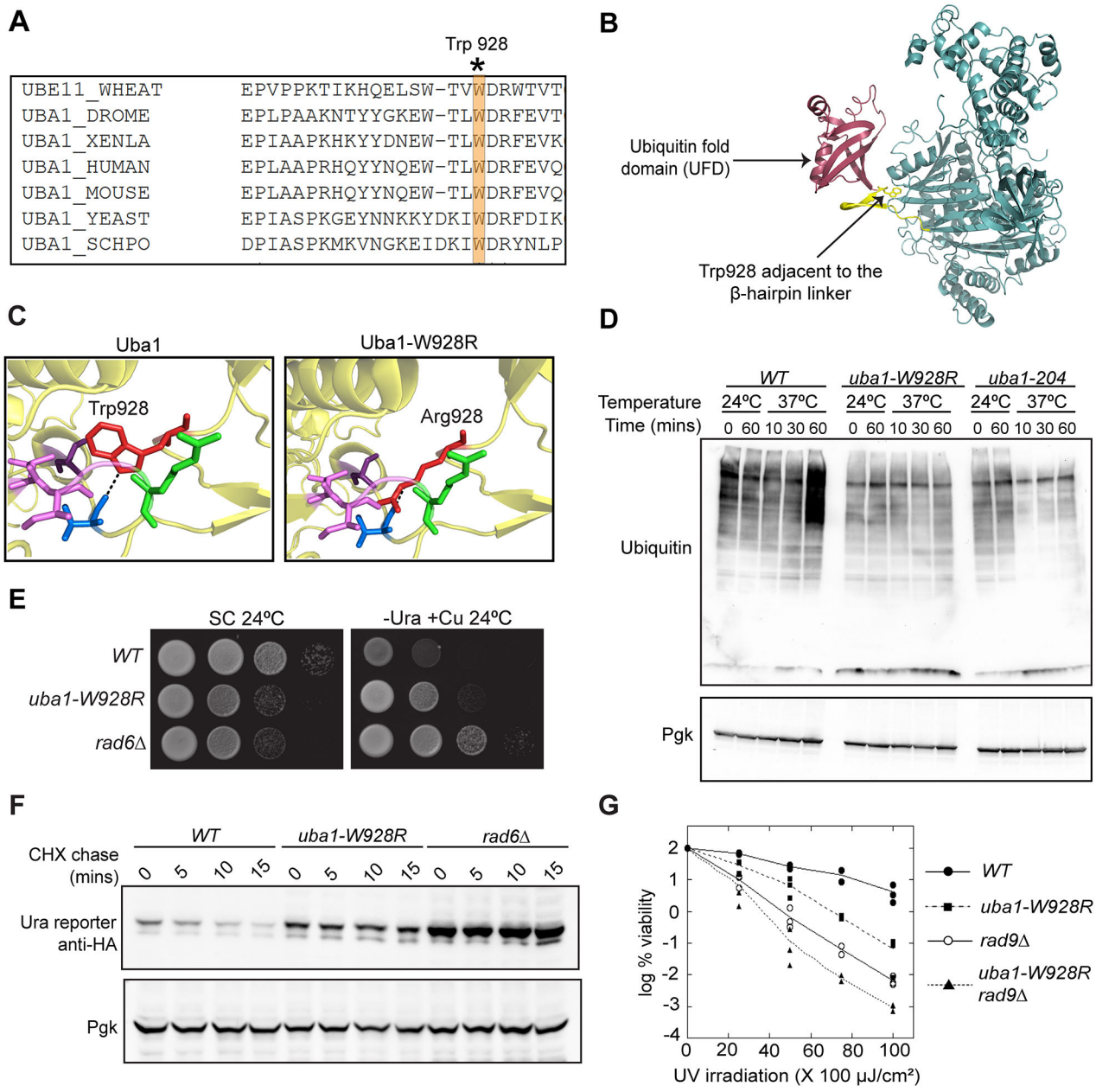

Fig. 2. *uba1-W928R* results in a pleiotropic phenotype. (A) Alignment of Uba1 protein sequences from wheat, *D. melanogaster*, *X. laevis*, human, mouse, *S. cerevisiae and S. pombe*. (B) The *S. cerevisiae* Uba1 structure (PDB 3CMM) (Lee and Schindelin, 2008). W928 is shown in stick representation. The linker region (yellow) of Uba1 acts as a hinge between the UFD E2 binding domain (magenta) and the catalytic domains (cyan). Note that W928 locks the hinge domain onto the catalytic domain. (C) PDB 3CMM showing W928 in stick representation in red (left panel). W928 is anchored into a hydrophobic pocket consisting of residues Val585, P580 and I578 (purple) on the active adenylation domain and forms a hydrogen bond with Thr583 (blue). The right panel shows changes in the structure when W928 is replaced by an arginine reisdue using the mutagenesis tool in Pymol (structure shown has the least steric hindrance among the 19 W928R rotamers). (D) Immunoblot analysis for ubiquitin in the *WT* (KT1113), *uba1-W928R* (KT3474) and *uba1-204* (KT3591) strains grown at 24°C and 37°C for the indicated times. Pgk1 was used as the loading control. (E) Serial dilution of *WT* (KT3817), *uba1-W928R* (KT3824) and *rad6*Δ (KT3900) strains expressing a *URA3* reporter gene with an N-terminal degron sequence on synthetic complete medium and medium lacking uracil with 100 µM copper (-Ura +Cu) to induce the *URA3* reporter gene. (F) Cycloheximide chase reactions to measure the turnover of a HA-tagged *URA3* reporter protein with an N-terminal degron sequence in *WT* (KT3817), *uba1-W928R* (KT3824) and *rad6*Δ (KT3900) strains. Immunoblots were probed with anti-HA antibody and Pgk1 was used as the loading control. (G) Quantification of viable cells for *WT* (KT1112), *uba1-W928R* (KT3475), *rad9*Δ (KT1679), *uba1-W928R rad9*Δ (KT3493) strains after UV irradiation. Individual data points from three independent experiments are plotted with the average trend line.

and *uba1-W928R mad1*Δ cells (Fig. 3C), indicating that the mitotic delay does not result from a failure to terminate the SAC.

The mitotic spindle lengths inferred from distances between the two spindle pole bodies are longer for *uba1-W928R* cells than for WT cells. To confirm that the spindle pole body distances accurately reflect spindle length, we performed live-cell microscopy on *uba1-W928R* strains expressing GFP-tagged tubulin. Consistent with the increased distances between spindle pole bodies, we observed that *uba1-W928R* cells show abnormally long spindles (Fig. 3D). The average spindle length at late anaphase, just before spindle disassembly, is 6.5 µm for the *WT* (n=5), compared to 11.2 µm for the *uba1-W938R* mutant (n=5). We followed spindle

Journal of Cell Science (2018) 131, jcs217620. doi:10.1242/jcs.217620

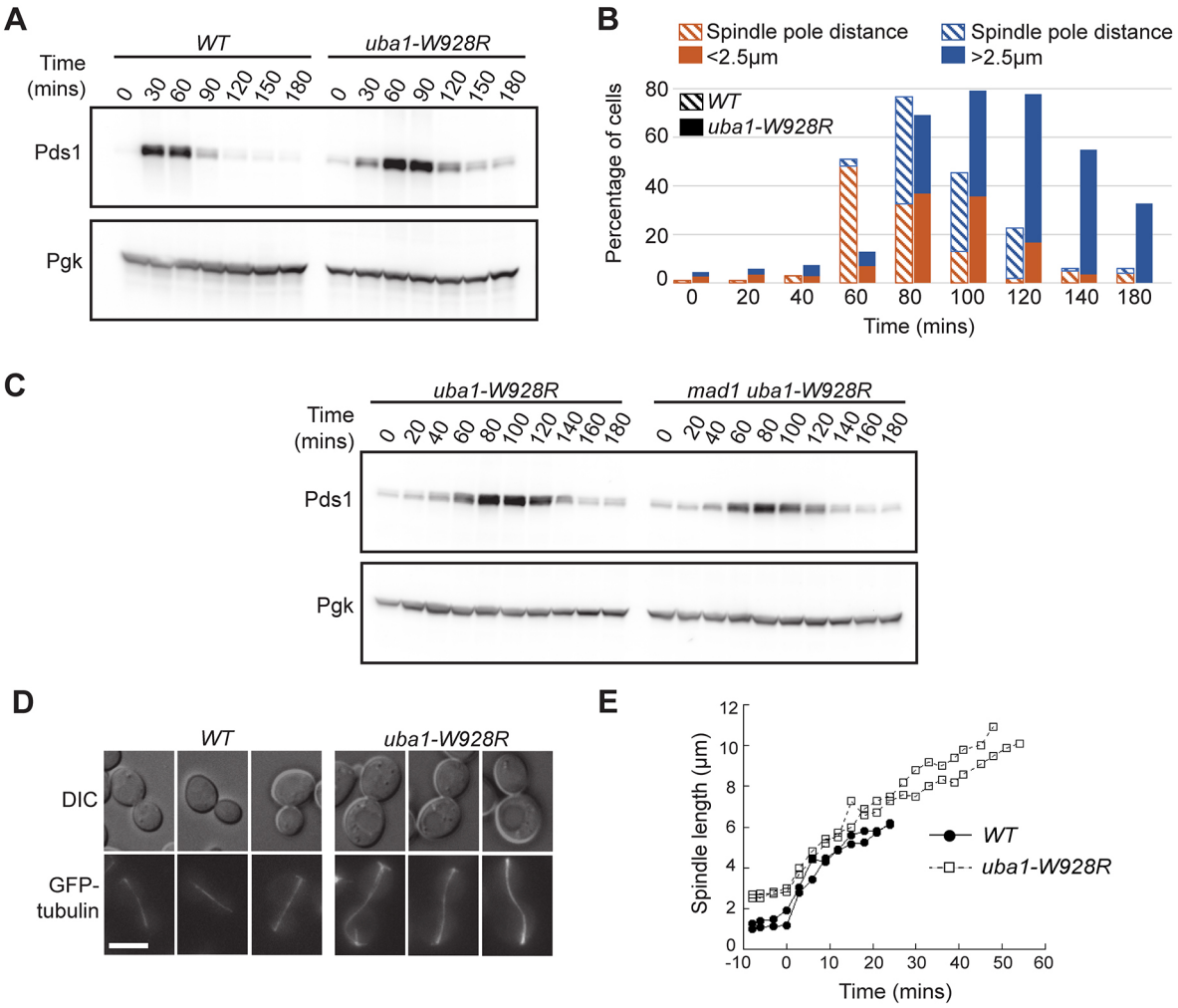

Fig. 3. *uba1-W928R* mutants exhibit a mitotic cell cycle delay. (A) Immunoblot analysis of *WT* (KT3319) and *uba1-W928R* (KT3487) strains expressing Myc-tagged Pds1. Protein extracts were prepared at the indicated time points, post release from α- factor. Pgk1 was used as the loading control. (B) Analysis of distance between spindle pole bodies in *WT* (KT3319) (striped) and *uba1-W928R* (KT3487) (filled) strains expressing GFP-tagged Spc42, after release from α-factor. The percentages of cells with short spindles (orange) or long spindles (blue) are plotted for the respective time points (n>100). (C) Immunoblot analysis of *uba1-W928R* (KT3487) and *mad1 uba1-W928R* (KT3614) strains as in A. (D) Fluorescence microscopy images of *WT* and *uba1-W928R* (RR103) mutant cells expressing GFP-tagged tubulin. Scale bar: 5 μm. (E) Spindle lengths at 3 min intervals in *WT* and *uba1-W928R* mutant cells from the start of elongation to spindle breakdown (n=2).

dynamics in individual cells by time-lapse microscopy and found that spindle disassembly is delayed in *uba1-W928R* (Fig. 3D, Movies 1 and 2). The average time between anaphase onset and spindle breakdown is 18 min for the *WT*, compared to 51 min for *uba1-W928R* cells. The spindles of only two of five *uba1-W928R* cells disassembled by 60 min.

This increase in spindle length may be due, in part, to an increase in cell size. However, we note that more than 10% of *uba1-W928R* cells have curved spindles (Fig. 3D), indicating that spindle disassembly may be influenced by *uba1-W928R*. Microtubule motor proteins are required to scale the anaphase spindle length to the cell length (Straight et al., 1998; Rizk et al., 2014). Similar to what is seen in *uba1-W928R*, cells containing mutations/deletions in the kinesin-related motor protein Kip3 exhibit delayed cell cycle progression through anaphase and display abnormally long anaphase spindles (Straight et al., 1998; Rizk et al., 2014). *kip3* mutants are also synthetic lethal with *cin8*, which encodes another kinesin motor protein (Pan et al., 2004). We tested for genetic interactions between *uba1-W928R* and mutations in microtubule motor genes, *DYN1*, *CIN8*, *KIP2*, *KIP3*, *KIP1* and *KAR3*. The most striking genetic interaction that we observed was synthetic lethality between *cin8* and *uba1-W928R* (Table S2). *cin8* mutations have been reported to interact genetically with many mutants, but the phenotypic similarity of *kip3* and *uba1-W928R*, and the *cin8 uba1-W928R* synthetic lethality, are consistent with the possibility that ubiquitylation directly or indirectly influences the activity of Kip3. Taken together, these results suggest that both defective motor protein function and slower degradation of Pds1 may contribute to the mitotic cell cycle delay exhibited by *uba1-W928R*.

uba1-W928R suppresses *ipl1-2* partly by increasing Ipl1 protein level and stability

Given that *uba1-W928R* mutants are defective in protein ubiquitylation and degradation via the N-end rule pathway, a likely explanation for the *ipl1-2* suppression phenotype is that the Ipl1 protein is stabilized in the *uba1-W928R* mutant. To test this hypothesis, we first assayed the phosphorylation state of histone H3 S10 (H3-S10), a known substrate of Ipl1 and Glc7 (Hsu et al., 2000).

Journal of Cell Science (2018) 131, jcs217620. doi:10.1242/jcs.217620

As a control, we also tested the phosphorylation state of H3-S10 in the *glc7-127* mutant, which restores H3-S10 phosphorylation in an *ipl1-2* mutant (Hsu et al., 2000). The *uba1-W928R* mutation in the *ipl1-2* strain raises H3-S10 phosphorylation to levels that are comparable to those in of *WT* (Fig. 4A). The restoration seen with *uba1-W928R* is less effective than that seen with *glc7-127*, consistent with the fact that *glc7-127* is a much stronger *ipl1-2* suppressor. The partial restoration of H3-S10 phosphorylation by *uba1-W928R* is consistent with the possibility that this mutation either increases Ipl1 kinase activity and/or reduces the opposing Glc7 phosphatase activity.

To determine whether *uba1-W928R* increases Ipl1 protein levels, we tagged the *IPL1* and *ipl1-2* loci with a 13× Myc C-terminal epitope (*13Xmyc*) and confirmed that the *ipl1-2-13Xmyc* strain has a similar profile of temperature sensitivity to the untagged *ipl1-2* mutant (Fig. S3A). Ipl1 and Ipl1-2 protein levels are increased 2.5- to 3-fold in the *uba1-W928R* mutant (Fig. 4B). The half-life of Ipl1-2–13Xmyc is 1.5 h in the *UBA1*$^{+}$ strain but more than 4 h in the *uba1-W928R* mutant background (Fig. 4D). To test whether an increase in Ipl1 protein level is sufficient to suppress *ipl1-2*, we expressed Ipl1 or Ipl1-2 from the galactose-inducible *GAL1* promoter in an *ipl1-2* strain and assessed growth at high temperatures. We observed that increased protein levels of either Ipl1 or Ipl1-2 allowed growth of *ipl1-2* cells even at 37°C (Fig. 4C, upper panel). The *ipl1-2* strain expressing Ipl1-2 from the *GAL1* promoter grows well on galactose medium but not on glucose medium, when expression is greatly reduced. Interestingly, expression of Ipl1 from the *GAL1* promoter fully suppresses the temperature sensitivity of *ipl1-2* even on glucose medium, suggesting that only a low level of Ipl1 is sufficient to suppress *ipl1-2* (Fig. 4C, lower panel). Taken together, these results suggest that *uba1-W928R* suppresses *ipl1-2* at least in part by stabilizing the

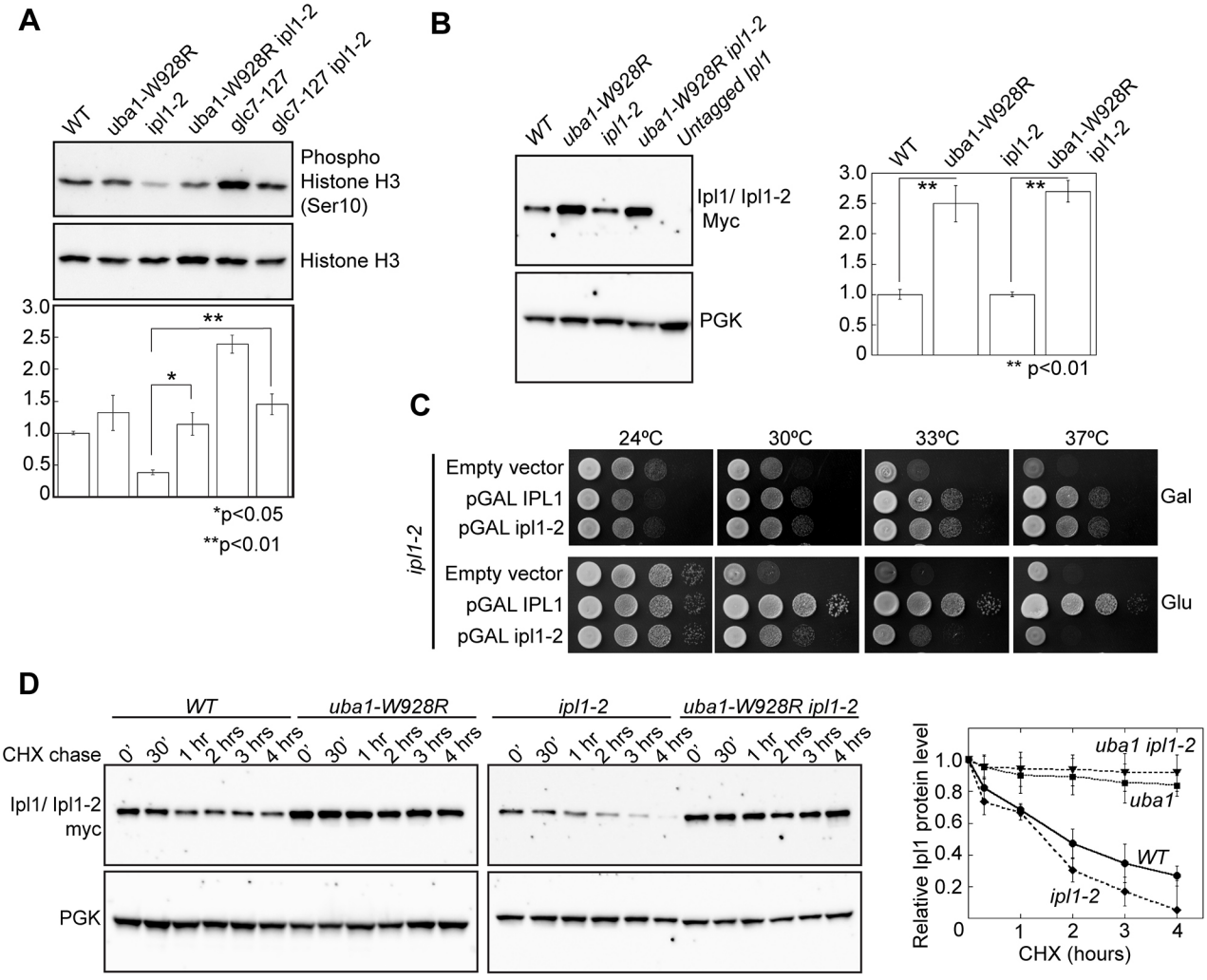

Fig. 4. The *uba1-W928R* mutation partially restores phosphorylation of Ipl1 substrate and H3-S10, and increases Ipl1 protein stability. (A) Protein extracts of *WT* (KT1113), *ipl1-2* (KT1829), *uba1-W928R* (KT3474), *ipl1-2 uba1-W928R* (KT3476), *glc7-127* (KT1967) and *ipl1-2 glc7-127* (KT1968) strains were probed with anti-phospho-H3-S10 antibody and signal intensities were calculated relative to total histone H3. (B) Immunoblot analysis of strains expressing Myc-tagged Ipl1 or Ipl1-2; levels in *WT* (KT3383), *uba1-W928R* (KT3482), *ipl1-2* (RR36), *ipl1-2 uba1-W928R* (RR39). Ipl1-13Myc and Ipl1-2 13Myc were calculated relative to the loading control (Pgk1). (C) Serial dilution of *ipl1-2* (KT1829) strain transformed with the indicated vectors on synthetic medium lacking uracil and containing either galactose (Gal, upper panel) or glucose (Glu, lower panel). Cultures were allowed to grow for 48 h at the indicated temperatures prior to imaging. (D) Cycloheximide chase analysis for Ipl1 turnover (left panel) and Ipl1-2 turnover (right panel) in *WT* (KT3383), *uba1-W928R* (KT3482), *ipl1-2* (RR36), *ipl1-2 uba1-W928R* (RR39) strains expressing Myc-tagged Ipl1 or Ipl1-2. Relative levels of Ipl1 and Ipl1-2 protein were quantified using Pgk1 as the loading control (lower panel) and plotted against chase time (extreme right panel). Quantitative results represent mean±s.d. for three independent experiments. **P*<0.05; ***P*<0.01 (two-tailed *t*-test).

Journal of Cell Science (2018) 131, jcs217620. doi:10.1242/jcs.217620

Ipl1-2 protein and, thus, increasing its protein level and activity. Consistent with this, we observe that Ipl1-2 accumulates upon proteasome inhibition (Fig. S3B).

uba1-W928R influences Glc7 localization and function

The elevation of Ipl1-2 levels due to *uba1-W928R* could account entirely for the *ipl1-2* suppression phenotype. However, we observe that *uba1-W928R* exhibits strong genetic interactions with *glc7* mutants (see below), suggesting the possibility that ubiquitylation affects Glc7 function. To test this, we first determined Glc7 protein levels in *uba1-W928R* strains. Unlike Ipl1, Glc7 protein levels are not elevated in *uba1-W928R*, even after treatment with MG132, which blocks proteasomal degradation (Fig. 5A). Consistent with these observations, Glc7 protein stability remains unchanged in the *uba1-W928R* mutant (Fig. 5B).

Glc7 mutations causing reduced activity are known to suppress *ipl1-2*, presumably by restoring the balance of phosphatase-to-kinase activity (Hsu et al., 2000). Even though Glc7 protein levels are unchanged in the *uba1-W928R* mutant, we sought to determine whether Glc7 is functionally compromised. We first analyzed meiotic progeny of crosses between *uba1-W928R* and two *glc7* mutant strains (*glc7-127* and *glc7-S99L*), which were shown previously to suppress *ipl1-2* (Hsu et al., 2000; Robinson et al., 2012). *uba1-W928R glc7* double mutants are very slow growing, failing to form viable macro colonies in 3 days (Fig. 5C). This could result from the increase in Ipl1 levels, which in the absence of fully functional Glc7 would lead to loss of cell growth and/or viability. If this were the case, then decreasing Ipl1 activity in the *uba1-W928R glc7* mutant should alleviate the growth defect. To test this, we compared growth rates of *uba1-W928R glc7-127* spore clones, with or without the *ipl1-2* mutant allele. Ipl1-2 is known to have reduced kinase activity at 24°C, the temperature at which the spore clones were incubated (Hsu et al., 2000). No difference in growth rates were noted for *uba1-W928R glc7-127* mutants, irrespective of their *IPL1* genotype (Fig. 5D), arguing that the slow growth of *uba1-W928R glc7* mutant strains is independent of Ipl1 activity.

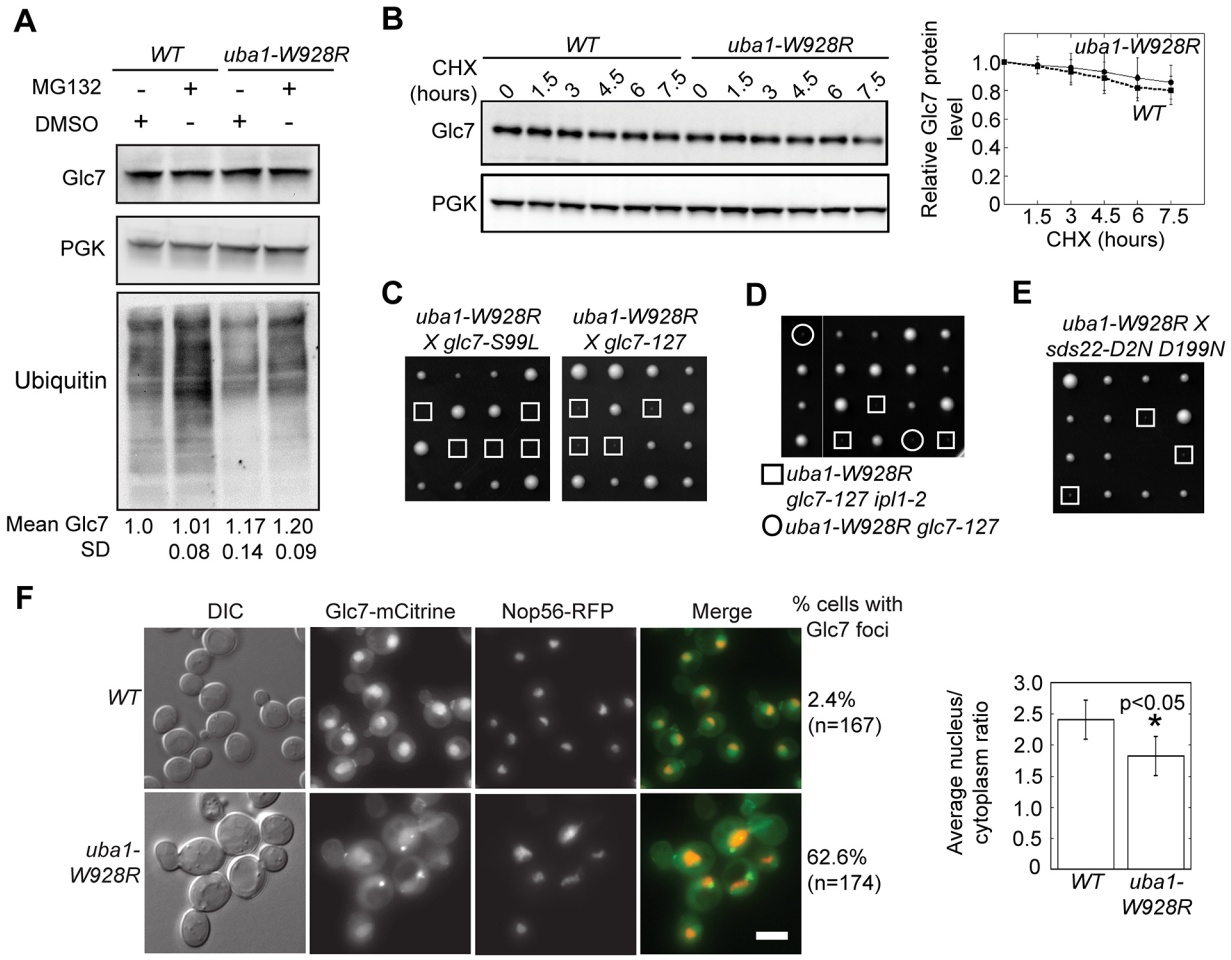

Fig. 5. *uba1-W928R* is synthetic lethal with *glc7* mutations and causes formation of Glc7 foci, but does not affect Glc7 protein level. (A) Immunoblot analysis of extracts from *WT* (KT3502) and *uba1-W928R* (KT3532) strains treated with DMSO or the proteasome inhibitor MG132 (75 µM), probed for Glc7 and total ubiquitin. Pgk1 is used as the loading control. Mean±s.d. levels from three independent experiments are denoted below the ubiquitin blot. (B) Cycloheximide chase analysis for Glc7 turnover in *WT* (KT2420) and *uba1-W928R* (KT3525) strains. Relative Glc7 protein level was quantified using Pgk1 as the loading control and plotted against chase time (right panel). Results are mean±s.d. for four immunoblots (two biological replicates). (C) Meiotic progeny of crosses between *uba1-W928R* and *glc7* mutants. Each column contains four haploid spore clones of a single meiosis (tetrad). Boxes identify the *uba1-W928R* double mutants. (D) Meiotic progeny of a cross between *ipl1-2 uba1-W928R* and *glc7-127* mutant strains. A key to the genotypes is shown below the panel. (E) Meiotic progeny of a cross between *uba1-W928R* and *sds22* mutant. Boxes identify the *uba1-W928R sds22-D2N D199N* double mutants. (F) Glc7–mCitrine was imaged in *WT* (KT3877) and *uba1-W928R* mutant (KT3880) cells. Scale bar: 5 µm. Cells possessing Glc7 foci were counted and the percentage is indicated on the right. A quantitative analysis of the ratio of nuclear-to-cytoplasmic fluorescence of Glc7–mCitrine in *WT* and *uba1-W928R* cells is shown on the right panel. Results are mean±s.d. for 167 *WT* and 174 *uba1-W928R* cells (two biological replicates).

Journal of Cell Science (2018) 131, jcs217620. doi:10.1242/jcs.217620

These observations are more consistent with the hypothesis that some aspect of Glc7 function is impaired in *uba1-W928R* mutants.

Synthetic lethality between *uba1-W928R* and *glc7* mutations could be explained if proper Glc7 function requires a ubiquitylation-dependent process. In this scenario, reduced ubiquitylation in the *uba1-W928R* mutant would negatively impact on Glc7 function, and further impairment due to a *glc7* mutation would lead to the inviability of the *uba1-W928R glc7* double mutant. If this were the case, mutations in positive regulators of Glc7 also should show synthetic growth defects with *uba1-W928R*. To test this, we analyzed meiotic progeny of a cross between an *sds22-D2N D199N* mutant strain that was isolated in an *ipl1-2* suppression screen (Robinson et al., 2012) and *uba1-W928R*. Sds22 is a leucine-rich repeat protein and an essential positive regulator of Glc7 (MacKelvie et al., 1995; Peggie et al., 2002; Pedelini et al., 2007). As observed with *glc7* mutants, the *sds22-D2N D199N* mutant strain also exhibits strong negative genetic interactions with *uba1-W928R* (Fig. 5E), further strengthening the hypothesis that some aspect of Glc7 function is regulated by ubiquitylation.

Previously characterized *ipl1-2* suppressors that act by compromising Glc7 function, such as *sds22-6*, *ypi1-GFP*, *cdc48-3* and *shp1*^{ts}, either reduce the nuclear-to-cytoplasmic ratio of Glc7 or cause Glc7 aggregation (Pedelini et al., 2007; Bharucha et al., 2008; Cheng and Chen, 2010, 2015; Robinson et al., 2012). We examined *WT* and *uba1-W928R* cells expressing Glc7–mCitrine by fluorescence microscopy. We observed that the Glc7 nuclear-to-cytoplasmic ratio is significantly reduced in *uba1-W928R* cells (Fig. 5F). More strikingly, 62% of the *uba1-W928R* cells show bright Glc7 foci in the nucleus. The average intensity of these spots is 2-fold higher than the nuclear Glc7 fluorescence and 4.5-fold higher than Glc7 fluorescence in the cytoplasm. 97% of Glc7 foci are located adjacent to, but not overlapping the area occupied by the nucleolar protein, Nop56 (Fig. 5F; Fig. S4A). We also observed that the percentage of cells possessing Glc7 foci increases significantly when *uba1-W928R* cells are shifted from 24°C to restrictive temperatures. 73% of these cells show foci when shifted to 33°C for 2 h and 85% of *uba1-W928R* cells show bright Glc7 foci when cultured at 14°C overnight (Figs S4B,C). Since Glc7 function and localization are perturbed in the *uba1-W928R* mutant, some aspect of Glc7 function is likely to be dependent on ubiquitin.

E2 ubiquitin-conjugating enzymes affect Ipl1–Glc7 function

The sensitivity of *uba1-W928R* strains to radiation and their defect in the N-end rule degradation pathway (Fig. 2F,G) suggest that the E2 Rad6 is not properly thioesterified to ubiquitin in *uba1-W928R* cells. To identify additional E2 ubiquitin-conjugating enzyme(s) that may be impacted by *uba1-W928R*, we tested mutations in nine of the eleven E2 ubiquitin-conjugating enzymes for traits similar to those found in *uba1-W928R* strains. Gene deletions were used for the non-essential E2 enzymes Rad6, Ubc4, Ubc5, Ubc7, Ubc8, Pex4, Ubc11 and Ubc13. The polyubiquitylation-defective *cdc34*^{tm} mutant (Cocklin et al., 2011; Lass et al., 2011) was used for the essential E2 enzyme Cdc34 (which associates with SCF E3 ligases). Each of these mutations was combined with either *ipl1-2* or *glc7-127* and assayed for suppression of temperature sensitivity or a synthetic growth phenotype, respectively.

The majority of the E2 deletion mutations do not suppress *ipl1-2* (Fig. S5A), nor do they confer a slow growth phenotype with *glc7-127* (Fig. S5B). Only two E2 enzyme mutations, *cdc34*^{tm} and *ubc4*Δ, suppress *ipl1-2* (Fig. 6A). We observed very weak *ipl1-2* suppression by *rad6*Δ (previously reported in Latham et al., 2011). Interestingly, *uba1-W928R* is a better *ipl1-2* suppressor than either *cdc34*^{tm} or *ubc4*Δ (Fig. 6A), suggesting that suppression of *ipl1-2* by *uba1-W928R* is conferred by defects in more than one E2 enzyme. Similarly, only *rad6*Δ and *cdc34*^{tm} confer a slow growth phenotype with *glc7-127* (Fig. 6B). While the *cdc34*^{tm} mutation suppresses *ipl1-2* and also displays genetic interaction with *glc7-127*, the *ubc4*Δ mutant suppresses *ipl1-2* but does not show any additive growth defects with *glc7-127* (Fig. S5B). Conversely, the *rad6*Δ mutation exhibits strong growth defects in combination with *glc7-127*, but is a very poor *ipl1-2* suppressor. Thus, our genetic evidence shows that perturbations in the activities of particular

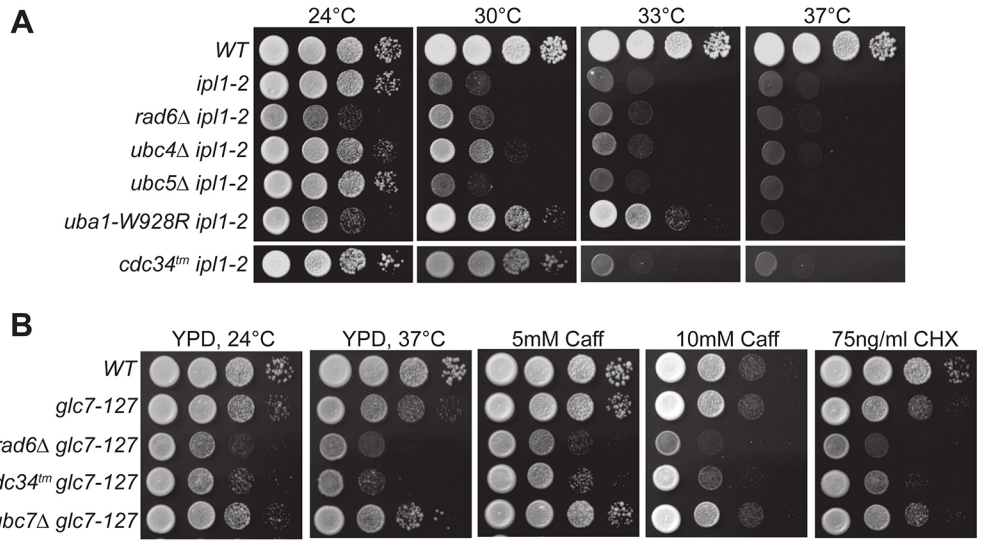

Fig. 6. E2 enzyme mutations suppress *ipl1-2* and show genetic interaction with *glc7-127*. (A) Cultures of *WT* (KT1113), *ipl1-2* (KT1829), *rad6*Δ *ipl1-2* (RR135), *ubc4 ipl1-2* (RR223), *ubc5*Δ *ipl1-2* (RR225), *uba1-W928R ipl1-2* (KT3476) and *cdc34*^{tm} *ipl1-2* (KT3807) strains were serially diluted onto rich medium (YPD) and imaged after 40 h at the indicated temperatures. *ubc5*Δ serves as a negative control for *ipl1-2* suppression. (B) Cultures of *WT* (KT1113), *glc7-127* (KT1967), *rad6*Δ *glc7-127* (KT3791), *cdc34*^{tm} *glc7-127* (RR267) and *ubc7*Δ *glc7-127* (RR259) strains were serially diluted onto rich medium (YPD) at 24°C/37°C or in medium containing caffeine or cycloheximide (CHX) at 24°C and imaged after 40 h of incubation. *ubc7*Δ serves as a negative control for synthetic growth defects with *glc7-127*.

Journal of Cell Science (2018) 131, jcs217620. doi:10.1242/jcs.217620

E2 enzymes lead to distinct effects on Ipl1 and Glc7 function, suggesting the existence of multiple independent ubiquitin-dependent pathways that influence Ipl1 and Glc7 activities.

A subset of *uba1-W928R* traits is observed in the *rad6*Δ and *cdc34*^{tm} mutants

uba1-W928R confers several distinct growth traits, including sensitivity to low and high temperatures, caffeine, CsCl, UV radiation, and resistance to LiCl (Fig. 1). Of the E2 enzyme mutants tested, only *rad6*Δ and *cdc34*^{tm} confer similar phenotypes to *uba1-W928R* (Fig. S6A). Moreover, as shown in Fig. 6A,B, genetic interaction of *rad6*Δ and *cdc34*^{tm} with *glc7-127* and the *ipl1-2* suppression by *cdc34*^{tm} resemble those caused by *uba1-W928R*. Since *rad6*Δ and *cdc34*^{tm} mutations result in multiple growth defects similar to those observed for *uba1-W928R*, it is plausible that such traits of *uba1-W928R* may be due to alteration of interactions with Rad6 and/or Cdc34. As shown in Fig. 6B, the single *rad6*Δ and *cdc34*^{tm} mutations confer slow growth with *glc7-127*, but this genetic interaction is not as strong as the synthetic lethality of *uba1-W928R* and *glc7-127*. We reasoned that if *uba1-W928R* fails to interact normally with both *rad6*Δ and *cdc34*^{tm}, then the *rad6*Δ *cdc34*^{tm} double mutant should show synthetic lethality with *glc7-127*. To test this, we assayed growth of meiotic progeny from diploid strains heterozygous for *rad6*Δ, *cdc34*^{tm} and *glc7-127*. The *rad6*Δ *cdc34*^{tm} *glc7-127* triple mutants grow very slowly (Fig. 7A). *rad6*Δ *cdc34*^{tm} mutants also give rise to small colonies, but these are significantly larger than those formed by the *rad6*Δ *cdc34*^{tm} *glc7-127* triple mutants (Fig. 7B). These results suggest that Rad6 and Cdc34 could be the key E2 enzymes acting downstream of Uba1 to affect Glc7 function.

Another trait conferred by *uba1-W928R* is the accumulation of bright Glc7 nuclear foci (Fig. 5F). To determine whether *rad6*Δ or *cdc34*^{tm} mutants also influence Glc7 localization, we examined Glc7–mCitrine fluorescence in *cdc34*^{tm} and *rad6*Δ strains. Bright foci of Glc7–mCitrine were observed in 68% of the *cdc34*^{tm} cells (Fig. 7C). The foci are located close to or overlapping the area of nucleolar Nop65–mRFP fluorescence, as observed in *uba1-W928R* mutant cells. We note that the *uba1-W928R cdc34*^{tm} double mutant

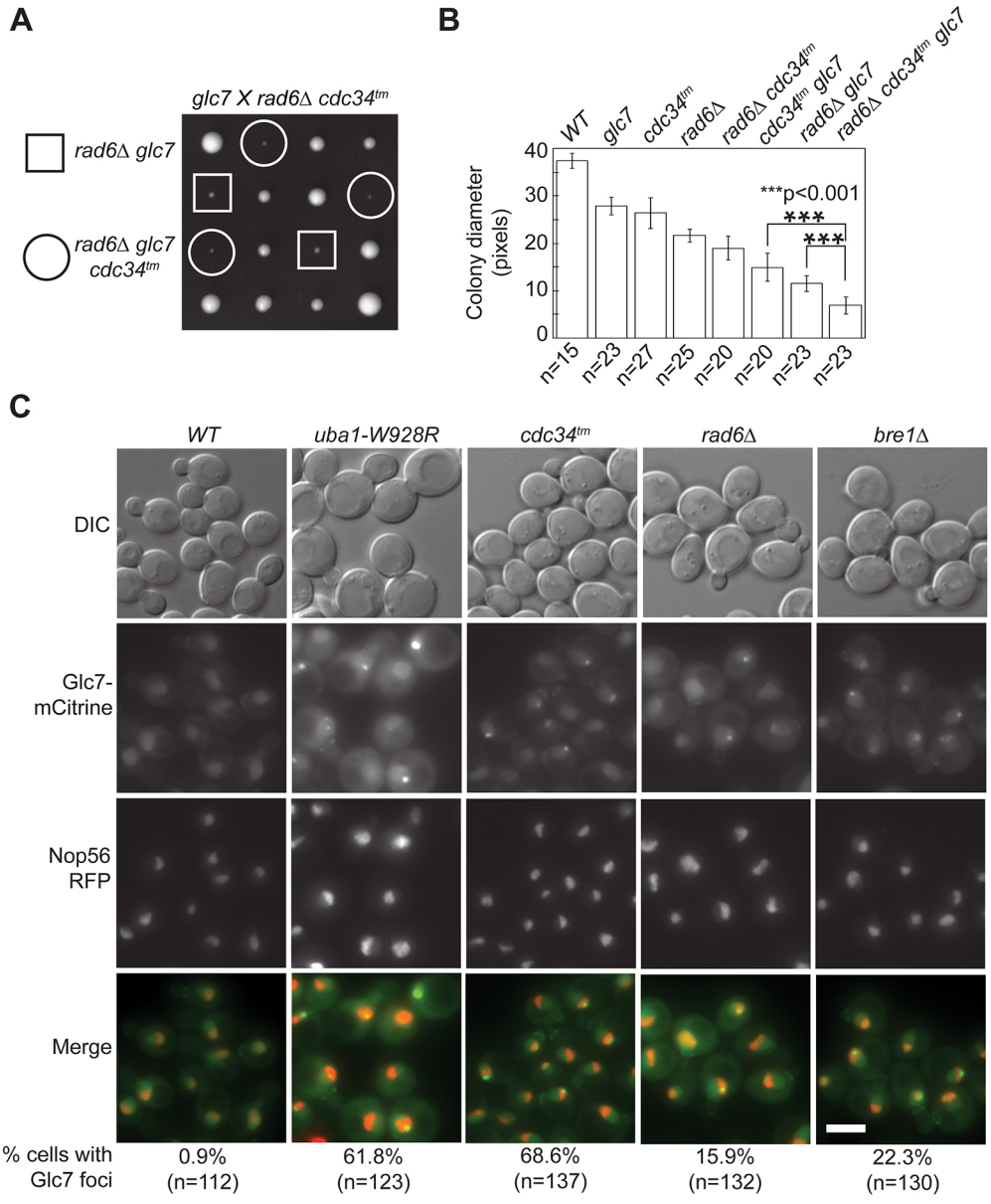

Fig. 7. Impairment of Rad6, Cdc34 and Bre1 influence Glc7 localization and function. (A) Meiotic progeny of crosses between *glc7-127* (*glc7* in figure) (KT1967) and *rad6*Δ *cdc34*^{tm} (RR284). Each column contains four haploid spore clones of a single meiosis (tetrad). Boxes identify the *rad6*Δ *glc7-127* double mutants. Circles identify *glc7-127 rad6*Δ *cdc34*^{tm} triple mutants. (B) Quantification of colony diameter of haploid spores of indicated genotypes. Results are mean±s.d. for diameter measurements of the indicated number of spore colonies (*n*) for each genotype. (C) Fluorescence images of Glc7–mCitrine and Nop56–mRFP in *WT* (KT3877), *uba1-W928R* (KT3880), *cdc34*^{tm} (RR328), *rad6*Δ (RR330) and *bre1*Δ (RR332) cells. The percentage of cells possessing Glc7 foci is indicated at the bottom. Scale bar: 5 µm.

Journal of Cell Science (2018) 131, jcs217620. doi:10.1242/jcs.217620

does not show enhancement of these defects (Fig. S6B). Glc7 foci are also present in cells lacking Rad6 or containing an alteration in its E3-binding partner, Bre1 (Fig. 7C). Taken together, these results indicate that Cdc34, Rad6 and Bre1 have previously unknown roles in regulating Glc7 localization and function. Suppression of *ipl1-2* by *rad6*Δ and *bre1*Δ (Latham et al., 2011) was thought to occur by indirectly affecting the kinetochore protein Dam1. Our results suggest that Rad6 and Bre1 also regulate Glc7, which could contribute to *ipl1-2* suppression.

DISCUSSION

We report here the identification and characterization of a novel *UBA1* allele, *uba1-W928R*, that suppresses *ipl1-2* defects. Ubiquitylation affects many pathways whose perturbation could result in suppression of *ipl1-2*. However, our observation that the *uba1-W928R* mutation partially restores histone H3-S10 phosphorylation in the *ipl1-2* mutant (Fig. 4A) indicates that the Ipl1–Glc7 kinase–phosphatase balance is altered. Since either an increase in Ipl1 activity or a decrease in Glc7 activity would result in both the restoration of HH3-S10 phosphorylation and suppression of *ipl1-2* growth defects, we were surprised to find that both Ipl1 and Glc7 are affected by the *uba1-W928R* mutation.

The *uba1-W928R* mutation increases the stability of WT Ipl1 and Ipl1-2 protein (Fig. 4B,D). Since increased expression of the Ipl1-2 protein restores temperature-independent growth to the *ipl1-2* strain, we conclude that the increase in Ipl1-2 protein levels due to *uba1-W928R* accounts for at least part of the suppression mechanism. This implies that one or more components of the CPC is ubiquitylated, and the simplest explanation is that Ipl1 is ubiquitylated and targeted for degradation. In metazoans, ubiquitylation regulates Aurora B by both proteasome- and non-proteasome-dependent mechanisms. A Cul3-based E3 ligase ubiquitylates Aurora B and targets it to the spindle midzone, which is necessary for coordinating faithful chromosome segregation and completion of cytokinesis (Sumara et al., 2007; Maerki et al., 2009). However, there is also evidence that ubiquitylation of Aurora B by the E3 ligase BARD1 targets it to the proteasome for degradation (Ryser et al., 2009). Aurora B is also known to bind to the APC/C subunits Cdh1 and Cdc20 *in vivo*, suggesting that Aurora B is degraded by the proteasome via the APC/C (Nguyen et al., 2005). Surprisingly, to date there has been no evidence for ubiquitin-dependent Ipl1 regulation in *S. cerevisiae*. Our work suggests that the E2 enzymes Cdc34 and Ubc4 are candidates to act downstream of *uba1-W928R* to regulate Ipl1, since *cdc34*^{tm} and *ubc4*Δ each suppresses *ipl1-2*. Cdc34 is the main, if not only, E2 enzyme partner of SCF ubiquitin–protein ligase complexes (Petroski and Deshaies, 2005). It colocalizes with β-tubulin on mitotic spindles during anaphase in mammalian cells and has well-defined roles in regulating cell cycle progression (Feldman et al., 1997; Kus, et al., 2004). Ubc4 is the key E2 that partners with Ubc1 to polyubiquitylate key cell cycle regulators targeted by the APC/C (Rodrigo-Brenni and Morgan, 2007). Moreover, Ubc4 has been reported to play an essential role in degradation of the mitotic cyclin Cdc13 in *Xenopus* and clam oocytes (Seino et al., 2003). Since *uba1-W928R* is a stronger *ipl1-2* suppressor than either of the single E2 mutants, multiple pathways may independently regulate Ipl1, similar to ubiquitylation of Aurora B in metazoans.

The *uba1-W928R* mutation also alters Glc7 localization, and cells containing this mutation in combination with one of several *glc7* mutations are very slow-growing or inviable. Since we ruled out the possibility that the genetic interactions are due to increased Ipl1 activity in the context of reduced phosphatase activity, we favor the possibility that ubiquitylation plays a positive role in Glc7 function. One potential role for ubiquitylation is in the context of Cdc48-dependent maturation of Glc7. Cheng and Chen (Cheng and Chen, 2015) showed that newly synthesized Glc7 aggregates in temperature-sensitive *cdc48-3* mutants at the restrictive temperature and in cells depleted of the Cdc48 adaptor protein Shp1. They also showed that Cdc48–Shp1 interacts transiently with Glc7, Sds22 and Ypi1, which together may be required to prevent misfolding of Glc7. Since substrates for the Cdc48 segregase are usually ubiquitylated, it is possible that ubiquitylation of Glc7, Sds22 and/or Ypi1 is necessary for the binding of Cdc48, which then acts as a foldase to prevent Glc7 misfolding. Interestingly, the PP1-related phosphatases Ppz1 and Ppz2 also interact transiently with Cdc48–Shp1 and require Cdc48–Shp1 chaperone function to prevent misfolding (Cheng and Chen, 2015). We note that *ppz1*Δ *ppz2*Δ double mutants are synthetic lethal with *uba1-W928R* (Fig. S7A), suggesting that *uba1-W928R* causes impaired Cdc48–Shp1 binding to multiple phosphatase substrates.

Although neither we nor Cheng and Chen (Cheng and Chen, 2015) were able to detect ubiquitylated forms of Glc7 by immunoblotting, both yeast Glc7 and human PP1 have been reported to be ubiquitylated at multiple lysine residues in proteomic screens for ubiquitylated proteins (Fig. S7C) (Wagner et al., 2011; Starita et al., 2012; Swaney et al., 2013). Also, the direct Cdc48–Shp1 substrate need not be Glc7. In global screens, the Glc7 regulators Ypi1, Shp1 and Cdc48 have been reported to be ubiquitylated *in vivo* (Swaney et al., 2013), but the function of this modification has not been investigated for any of these proteins. Sds22 protein levels are twice as high in *uba-W928R* mutants as in WT (Fig. S7B), suggesting that stability of Sds22 is determined by ubiquitylation. Therefore, given our results and that multiple components of the Glc7 maturation pathway are known to be ubiquitylated, we propose that ubiquitylation of Glc7 and/or its regulators influences Glc7 localization and activity.

Glc7 aggregation and reduced nuclear localization are hallmarks of mutations affecting genes in the Glc7 maturation pathway. *sds22-6*, *ypi1-GFP*, *cdc48-3* and *shp1*^{ts} mutants exhibit both nuclear and cytoplasmic Glc7 aggregates. However, the Glc7 foci observed in *uba1-W928R*, *rad6*Δ, *cdc34*^{tm} and *bre1*Δ cells are nuclear, adjacent to the nucleolar protein Nop56. One of our future goals is to determine whether the aggregates observed in *uba1-W928R* differ biochemically from those that form due to alteration of Glc7 regulatory proteins. This would inform us about the specific step(s) in Glc7 maturation that require ubiquitylation. It is possible that, while perturbation of the Glc7 regulatory pathway causes misfolding of newly synthesized Glc7 (Cheng and Chen, 2015), ubiquitylation may be required at a later step. Consistent with this, *uba1-W928R* cells exhibit nuclear Glc7 foci even after cycloheximide treatment (Fig. S7D).

As mentioned above, the E2 conjugating enzymes Rad6 and Cdc34 also influence Glc7. Mutations in *rad6* and *cdc34* show synthetic growth defects with *glc7-127* and cause Glc7 foci formation (Figs 6B and 7B). Although the principal function of Cdc34 is to regulate protein levels of SCF target substrates, it is also known to play a role in nuclear protein quality control, along with the San1 E3 ligase (Gardner et al., 2005). The bright Glc7 nuclear foci observed in the *cdc34*^{tm} mutant suggest that Cdc34 may be required for clearing misfolded nuclear Glc7, so that in its absence, Glc7 accumulates and forms foci. There has been no evidence to date for a role of Rad6 in protein quality control. Rad6 is known to partner with three RING E3 ligases, Rad18, Ubr1 and Bre1. The Rad6–Ubr1 pair polyubiquitylates N-end rule substrates (Dohmen et al., 1991) and, since we do not observe changes in Glc7 protein

Journal of Cell Science (2018) 131, jcs217620. doi:10.1242/jcs.217620

levels in the *uba1-W928R* mutant, it is unlikely that this pathway regulates Glc7 function. Along with Rad18, Rad6 specifically monoubiquitylates K164 on proliferating cell nuclear antigen (PCNA) to mediate repair of post-replicative DNA damage (Hoege et al., 2002). The Rad6–Bre1 pair monoubiquitylates histone H2B on K123 (equivalent to mammalian H2B K120), which in turn regulates histone H3K4 methylation and gene silencing (Wood et al., 2003). Interestingly, this H2B modification also affects mitosis, by indirectly reducing Ipl1-mediated phosphorylation of the kinetochore substrate Dam1 (Latham et al., 2011). Our data suggest a new role for Rad6–Bre1 in maintaining Glc7 localization. Both *rad6*Δ and *bre1*Δ accumulate Glc7 foci and show genetic interaction with the *glc7-127* mutant allele (Fig. 7C; Fig. S7E). Since the only known substrate of Bre1 (human RNF20 and RNF40) to date is histone H2B K123, this modification may indirectly affect Glc7 localization. Alternatively, Bre1 may have unidentified substrates beyond histone H2B (previously proposed in Turco et al., 2015).

In summary, our new *UBA1* allele illuminates two new mechanisms for ubiquitin-dependent regulation of the Ipl1–Glc7 balance in budding yeast, by affecting Ipl1 protein stability, and Glc7 localization and activity. Since yeast Glc7 is over 80% identical to mammalian PP1 and the essential function of Glc7 can be complemented by human PP1 isoforms (Gibbons et al., 2007), knowledge of ubiquitin-mediated regulation of Glc7 could provide novel mechanisms for modulation of PP1 in metazoans.

MATERIALS AND METHODS

Strains, media and general methods

The yeast strains used in this study are listed in Table S3 and are congenic to strain JC482 (Cannon and Tatchell, 1987). Yeast strains were grown on medium containing 1% yeast extract, 2% peptone, and 2% glucose (YPD) or synthetic complete (SC) medium (Sherman et al., 1986) or modifications of these media as stated. Filter sterilized 0.25M caffeine stock in H_2O (Sigma 68F-0817) was added to autoclaved rich medium and used for serial dilution tests. Strains were sporulated at 24°C on medium containing 0.1% yeast extract, 0.05% glucose and 1% potassium acetate. Yeast transformation, manipulation of *Escherichia coli*, and the preparation of bacterial growth medium were performed as described previously (Sherman et al., 1986). Tetrad dissection and analysis were performed as described previously (Rose et al., 1990). The Myc-tagged variants of *ipl1-2* and *SDS22* were generated by the method of Longtine (Longtine et al., 1998) with primers listed in Table S4. PCR products with the tagged alleles were introduced into the WT diploid strain KT1112/KT1113 by transformation. G418-resistant transformants were sporulated, and protein extracts from G418-resistant meiotic progeny were assayed for the presence of the tagged protein by immunoblotting. Strains containing deletions of E2 enzyme genes were made by using PCR to amplify deletion cassettes from genomic DNA of appropriate strains from the yeast deletion collection (Winzeler et al., 1999) and transforming the WT KT1112/KT1113 strain with the PCR products. Primers used are listed in Table S4. Chromosome III loss in diploids and segregation of GFP-tagged chromosome IV were assayed as described previously (Tatchell et al., 2011). The *rev100* mutant was isolated as elaborated previously (Tatchell et al., 2011; Robinson et al., 2012). To assay the sensitivity of yeast cells to UV light, cultures were grown to logarithmic phase at 24°C in YPD medium, plated onto YPD plates, exposed to UV irradiation in a CL-1000 Ultraviolet Crosslinker (UVP) and then incubated for 4 days at 24°C before counting colonies.

DNA manipulation and sequence analysis

The *E. coli* strain DH5α was used to amplify all plasmids. DH5α was grown in LB medium supplemented with ampicillin to select for plasmids. Transformation of chemically competent bacterial cells was as described previously (Sambrook et al., 1989). Restriction enzymes (Promega), DNA ligase (NEB), and high-fidelity DNA polymerase for PCR (Bio-Rad and Phenix) were used according to the manufacturer's instructions. Yeast genomic DNA was isolated using the YeastStar kit (Zymo Research), and yeast plasmid DNA was isolated using the Zymoprep kit (Zymo Research). Plasmids were purified from *E. coli* using the GenElute miniprep kit (Sigma-Aldrich). DNA restriction fragments were purified from agarose gel slices using the ZymoClean kit (Zymo Research).

Whole-genome sequence analysis

To identify the mutation responsible for suppression and slow growth, we carried out serial backcrosses of a *rev100* mutant strain to our unmutagenized parent strain and prepared genomic DNA from six *MATα rev100* ascosporal clones from the fourth backcross. Whole-genome sequence analysis on the pooled DNA was performed using the Illumina MiSeq. DNA libraries were prepared from 1 ng of genomic DNA using the Illumina Nextera XT kit (Illumina, Inc., San Diego, CA) according to the manufacturer's protocol. In brief, DNA was simultaneously fragmented and tagged with unique adapter sequences in a tagmentation reaction. A limited-cycle PCR reaction was used to amplify the insert DNA and add index sequences to both ends of the DNA. Libraries were analyzed on an Agilent Bioanalyzer 2100 HS DNA assay (Agilent Technologies, Santa Clara, CA) to determine average size. Libraries were normalized, pooled and denatured. A 1.0% library of 12.5 pM PhiX was spiked in as an internal control. The library pool was sequenced on an Illumina MiSeq, with a read length of 2×250 base pairs. Base calling and quality scoring were performed with Illumina Real Time Analysis software (RTA). Illumina MiSeq Reporter software was used to demultiplex reads, generate FASTQ files and align indexed reads to *S. cerevisiae* (saCer2). Alignment was performed using the Burrows–Wheeler aligner (BWA; https://arxiv.org/abs/1303.3997v2). Variants were then called in MiSeq Reporter using the Genome Analysis Toolkit (GATK).

Microscopy and cell cycle analysis

Live yeast cells from log phase cultures were placed on a 2% agarose pad and imaged using a CoolSNAP HQ charge-coupled device camera through an Olympus UPlanFl 100×1.3 NA objective. Filters from Chroma Technology were used to image cells expressing proteins tagged with mCitrine, mCherry and mRFP. SlideBook 6 software (Intelligent Imaging Innovations), was used to control camera acquisition, fluorescence filter wheels, and the *z*-axis stepping motor (Ludl Electronic Products). Fluorescence images (binned 2×2) were acquired in a series of *z*-axis planes (0.5 µm apart). For measuring fluorescence intensity, images in nine planes were converted into a *z*-axis projection and the maximum fluorescence in nine adjacent pixels was measured using ImageJ software. Distances between spindle pole bodies, lengths of spindles and diameter of spore clones were measured using the ImageJ software. For cell cycle analysis, overnight cultures were diluted 1:20 and grown to log phase at 24°C. Cultures were synchronized by addition of α-factor (0.1 mg/ml final concentration) and incubated for a further 2 h. Cells were collected by centrifugation at 200 ***g***, washed twice by centrifugation, and resuspended in YPD containing nocodazole (15 µg/ml final concentration) or DMSO. Aliquots were taken every 30 min for western blotting and every 20 min for microscopy. To study spindle dynamics, fluorescence microscopy of *WT* and *uba1-W928R* cells expressing GFP-tagged Spc42 was performed. Cells were synchronized using α-factor, released in fresh medium and aliquots were taken every 20 min for microscopy. Time-lapse microscopy to quantify spindle elongation rate was performed by imaging synchronized cells expressing Tub1–GFP every 3 min, and spindle lengths were measured using ImageJ.

Immunoblot analysis

Total protein extracts were prepared from yeast cultures in log phase grown at 24°C and shifted to restrictive temperature when indicated. For drug treatments, log phase cultures were split in half, followed by addition of DMSO/autoclaved water or the indicated concentration of drug [MG132 (75 µM), cycloheximide (200 µg/ml)] to the culture. Cells were collected and lysed in tricholoracetic acid using glass beads (Davis et al., 1993), and total protein extracts were electrophoresed on Tris-glycine gradient gels (Criterion; Bio-Rad Any kDa or 4–20%) or 12% SDS-PAGE gels. Gels were blotted onto nitrocellulose (Amersham Protran) or PVDF (Bio-Rad) for H3-S10 detection. Immunoblot analysis was performed as described

previously (Stuart et al., 1994). The following antibodies were used: anti-ubiquitin (1:1000, FK2, SMC-550 StressMarq Biosciences), anti-Myc (1:1000, 9E10; Evan et al. 1985), anti-GFP (1:2000, JL-8; Kozubowski et al. 2003), anti-HA (1:1000, 12CA5; Wilson et al. 1984), anti-Histone H3 (1:1000, ab1791, Abcam), anti-phospho-H3-S10 (1:1000, 06-570, EMD Millipore) with horseradish peroxidase (HRP)-conjugated secondary antibody (Bio-Rad 170-5046 and 170-5047) and subsequent detection using ECL reagents (Clarity Western Bio-Rad). The anti-Glc7 goat serum was a gift from Andreas Mayer, University of Lausanne, Switzerland. Protein levels were quantified from immunoblots using the ChemiDoc Touch imaging system with Image Lab 6.0 software (Bio-Rad). Anti-phosphoglycerate kinase (Pgk1) (Life Technologies) was used as a loading control. H3-Ser10 phosphorylation was detected as described in Tatchell et al. (2011).

Acknowledgements
We thank Alan Tartakoff (Case Western Reserve University) for the *NOP56-mRFP* strain, John Hanna (Harvard Medical School) for the *URA3* reporter-degron strain, Mark Goebl (Indiana University School of Medicine) for the *cdc34^{tm}* strain, Raymond Deshaies (Caltech) for the *uba1-204* strain and the *UBA1*-pRS306 plasmid and Sue Biggins (Fred Hutchinson Cancer Research Center) for the *IPL1-pGAL* plasmid.

Competing interests
The authors declare no competing or financial interests.

Author contributions
Conceptualization: L.C.R., K.T.; Methodology: R.R., P.P., L.C.R., K.T.; Validation: R.R., P.P., K.T.; Formal analysis: R.R., P.P., L.C.R., K.T.; Investigation: R.R., P.P., L.C.R., K.T.; Writing - original draft: R.R., K.T.; Writing - review & editing: R.R., L.C.R., K.T.; Visualization: R.R., K.T.; Supervision: L.C.R., K.T.; Project administration: L.C.R., K.T.; Funding acquisition: K.T.

Funding
The Department of Biochemistry and Molecular Biology (to K.T., L.C.R. and R.R.), the Research Core Facility (to K.T., L.C.R. and P.P.) and the Feist-Weiller Cancer Center (to K.T., L.C.R. and P.P.) at Louisiana State University Health Sciences Center-Shreveport supported this work. R.R. was supported by an Ike Muslow Predoctoral Fellowship awarded by the School of Graduate Studies, Louisiana State University Health Sciences Center, Shreveport.

Supplementary information
Supplementary information available online at
http://jcs.biologists.org/lookup/doi/10.1242/jcs.217620.supplemental

References
Albuquerque, C. P., Smolka, M. B., Payne, S. H., Bafna, V., Eng, J. and Zhou, H. (2008). A multidimensional chromatography technology for in-depth phosphoproteome analysis. *Mol. Cell. Proteomics* **7**, 1389-1396.

Ayusawa, D., Kaneda, S., Itoh, Y., Yasuda, H., Murakami, Y., Sugasawa, K., Hanaoka, F. and Seno, T. (1992). Complementation by a cloned human ubiquitin-activating enzyme E1 of the S-phase-arrested mouse FM3A cell mutant with thermolabile E1. *Cell Struct. Funct.* **17**, 113-122.

Bharucha, J. P., Larson, J. R., Gao, L., Daves, L. K. and Tatchell, K. (2008). Ypi1, a Positive Regulator of Nuclear Protein Phosphatase Type 1 Activity in Saccharomyces cerevisiae. *Mol. Biol. Cell* **19**, 1032-1045.

Biggins, S., Severin, F. F., Bhalla, N., Sassoon, I., Hyman, A. A. and Murray, A. W. (1999). The conserved protein kinase Ipl1 regulates microtubule binding to kinetochores in budding yeast. *Genes Dev.* **13**, 532-544.

Böhm, S. (2011). *The Cdc48 SHP1 Complex Mediates Cell Cycle Progression by Positive Regulation of Glc7. PhD thesis*, Ludwig-Marimilians-Universitat, Munich, Germany.

Bollen, M., Peti, W., Ragusa, M. J. and Beullens, M. (2010). The extended PP1 toolkit: designed to create specificity. *Trends Biochem. Sci.* **35**, 450-458.

Cannon, J. F. and Tatchell, K. (1987). Characterization of Saccharomyces cerevisiae genes encoding subunits of cyclic AMP-dependent protein kinase. *Mol. Cell. Biol.* **7**, 2653-2663.

Carmena, M., Wheelock, M., Funabiki, H. and Earnshaw, W. C. (2012). The chromosomal passenger complex (CPC): from easy rider to the godfather of mitosis. *Nat. Rev. Mol. Cell Biol.* **13**, 789-803.

Cejka, P., Vondrejs, V. and Storchova, Z. (2001). Dissection of the functions of the Saccharomyces cerevisiae RAD6 postreplicative repair group in mutagenesis and UV sensitivity. *Genetics* **159**, 953-963.

Chan, C. S. and Botstein, D. (1993). Isolation and characterization of chromosome-gain and increase-in- ploidy mutants in yeast. *Genetics* **135**, 677-691.

Chau, V., Tobias, J. W., Bachmair, A., Marriott, D., Ecker, D. J., Gonda, D. K. and Varshavsky, A. (1989). A multiubiquitin chain is confined to specific lysine in a targeted short-lived protein. *Science* **243**, 1576-1583.

Cheeseman, I. M., Anderson, S., Jwa, M., Green, E. M., Kang, J., Yates, J. R., III, Chan, C. S., Drubin, D. G. and Barnes, G. (2002). Phospho-regulation of kinetochore-microtubule attachments by the Aurora kinase Ipl1p. *Cell* **111**, 163-172.

Cheng, Y.-L. and Chen, R.-H. (2010). The AAA-ATPase Cdc48 and cofactor Shp1 promote chromosome bi-orientation by balancing Aurora B activity. *J. Cell Sci.* **123**, 2025-2034.

Cheng, Y.-L. and Chen, R.-H. (2015). Assembly and quality control of the protein phosphatase 1 holoenzyme involves the Cdc48-Shp1 chaperone. *J. Cell Sci.* **128**, 1180-1192.

Cocklin, R., Heyen, J., Larry, T., Tyers, M. and Goebl, M. (2011). New insight into the role of the Cdc34 ubiquitin-conjugating enzyme in cell cycle regulation via Ace2 and Sic1. *Genetics* **187**, 701-715.

Davis, N. G., Horecka, J. L. and Sprague, G. F. Jr. (1993). Cis- and trans-acting functions required for endocytosis of the yeast pheromone receptors. *J. Cell Biol.* **122**, 53-65.

Dohmen, R. J., Madura, K., Bartel, B. and Varshavsky, A. (1991). The N-end rule is mediated by the UBC2(RAD6) ubiquitin-conjugating enzyme. *Proc. Natl. Acad. Sci. USA* **88**, 7351-7355.

Eiteneuer, A., Seiler, J., Weith, M., Beullens, M., Lesage, B., Krenn, V., Musacchio, A., Bollen, M. and Meyer, H. (2014). Inhibitor-3 ensures bipolar mitotic spindle attachment by limiting association of SDS22 with kinetochore-bound protein phosphatase-1. *EMBO J.* **33**, 2704-2720.

Evan, G. I., Lewis, G. K., Ramsay, G. and Bishop, J. M. (1985). Isolation of monoclonal antibodies specific for human c-myc proto-oncogene product. *Mol. Cell. Biol.* **5**, 3610-3616.

Fang, N. N., Chan, G. T., Zhu, M., Comyn, S. A., Persaud, A., Deshaies, R. J., Rotin, D., Gsponer, J. and Mayor, T. (2014). Rsp5/Nedd4 is the main ubiquitin ligase that targets cytosolic misfolded proteins following heat stress. *Nat. Cell Biol.* **16**, 1227-1237.

Feldman, R. M., Correll, C. C., Kaplan, K. B. and Deshaies, R. J. (1997). A complex of Cdc4p, Skp1p, and Cdc53p/cullin catalyzes ubiquitination of the phosphorylated CDK inhibitor Sic1p. *Cell* **91**, 221-230.

Finley, D., Ciechanover, A. and Varshavsky, A. (1984). Thermolability of ubiquitin-activating enzyme from the mammalian cell cycle mutant ts85. *Cell* **37**, 43-55.

Finley, D., Ulrich, H. D., Sommer, T. and Kaiser, P. (2012). The ubiquitin-proteasome system of Saccharomyces cerevisiae. *Genetics* **192**, 319-360.

Gardner, R. G., Nelson, Z. W. and Gottschling, D. E. (2005). Degradation-mediated protein quality control in the nucleus. *Cell* **120**, 803-815.

Ghaboosi, N. and Deshaies, R. J. (2007). A conditional yeast E1 mutant blocks the ubiquitin-proteasome pathway and reveals a role for ubiquitin conjugates in targeting Rad23 to the proteasome. *Mol. Biol. Cell* **18**, 1953-1963.

Giannattasio, M., Lazzaro, F., Plevani, P. and Muzi-Falconi, M. (2005). The DNA damage checkpoint response requires histone H2B ubiquitination by Rad6-Bre1 and H3 methylation by Dot1. *J. Biol. Chem.* **280**, 9879-9886.

Gibbons, J. A., Kozubowski, L., Tatchell, K. and Shenolikar, S. (2007). Expression of human protein phosphatase-1 in Saccharomyces cerevisiae highlights the role of phosphatase isoforms in regulating eukaryotic functions. *J. Biol. Chem.* **282**, 21838-21847.

Hanna, J., Hathaway, N. A., Tone, Y., Crosas, B., Elsasser, S., Kirkpatrick, D. S., Leggett, D. S., Gygi, S. P., King, R. W. and Finley, D. (2006). Deubiquitinating enzyme Ubp6 functions noncatalytically to delay proteasomal degradation. *Cell* **127**, 99-111.

Hisamoto, N., Frederick, D. L., Sugimoto, K., Tatchell, K. and Matsumoto, K. (1995). The *EGP1* gene may be a positive regulator of protein phosphatase type 1 in the growth control of *Saccharomyces cerevisiae*. *Mol. Cell. Biol.* **15**, 3767-3776.

Hoege, C., Pfander, B., Moldovan, G. L., Pyrowolakis, G. and Jentsch, S. (2002). RAD6-dependent DNA repair is linked to modification of PCNA by ubiquitin and SUMO. *Nature* **419**, 135-141.

Holt, L. J., Tuch, B. B., Villen, J., Johnson, A. D., Gygi, S. P. and Morgan, D. O. (2009). Global analysis of Cdk1 substrate phosphorylation sites provides insights into evolution. *Science* **325**, 1682-1686.

Hsu, J.-Y., Sun, Z.-W., Li, X., Ruben, M., Tatchell, K., Bishop, D. K., Grushcow, J. M., Brame, C. J., Caldwell, J. A., Hunt, D. F. et al. (2000). Mitotic phosphorylation of histone H3 is governed by Ipl1/aurora kinase and Glc7p/PP1 phosphatase in budding yeast and nematodes. *Cell* **102**, 279-291.

Jin, L., Williamson, A., Banerjee, S., Philipp, I. and Rape, M. (2008). Mechanism of ubiquitin-chain formation by the human anaphase-promoting complex. *Cell* **133**, 653-665.

Jue, D., Sang, X., Lu, S., Dong, C., Zhao, Q., Chen, H. and Jia, L. (2015). Genome-wide identification, phylogenetic and expression analyses of the ubiquitin-conjugating enzyme gene family in maize. *PLoS ONE* **10**, e0143488.

Kelly, A. E., Ghenoiu, C., Xue, J. Z., Zierhut, C., Kimura, H. and Funabiki, H. (2010). Survivin reads phosphorylated histone H3 threonine 3 to activate the mitotic kinase Aurora B. *Science* **330**, 235-239.

Komander, D. and Rape, M. (2012). The ubiquitin code. *Annu. Rev. Biochem.* **81**, 203-229.

Kozubowski, L., Panek, H., Rosenthal, A., Bloecher, A., DeMarini, D. J. and Tatchell, K. (2003). A Bni4-Glc7 phosphatase complex that recruits chitin synthase to the site of bud emergence. *Mol. Biol. Cell* **14**, 26-39.
Kulka, R. G., Raboy, B., Schuster, R., Parag, H. A., Diamond, G., Ciechanover, A. and Marcus, M. (1988). A Chinese hamster cell cycle mutant arrested at G2 phase has a temperature-sensitive ubiquitin-activating enzyme, E1. *J. Biol. Chem.* **263**, 15726-15731.
Kus, B. M., Caldon, C. E., Andorn-Broza, R. and Edwards, A. M. (2004). Functional interaction of 13 yeast SCF complexes with a set of yeast E2 enzymes in vitro. *Proteins* **54**, 455-467.
Kulkarni, M. and Smith, H. E. (2008). E1 ubiquitin-activating enzyme UBA-1 plays multiple roles throughout C. elegans development. *PLoS Genet.* **4**, e1000131.
Lao, T., Chen, S. and Sang, N. (2012). Two mutations impair the stability and function of ubiquitin-activating enzyme (E1). *J. Cell. Physiol.* **227**, 1561-1568.
Lass, A., Cocklin, R., Scaglione, K. M., Skowyra, M., Korolev, S., Goebl, M. and Skowyra, D. (2011). The loop-less tmCdc34 E2 mutant defective in polyubiquitination in vitro and in vivo supports yeast growth in a manner dependent on Ubp14 and Cka2. *Cell Div.* **6**, 7.
Latham, J. A., Chosed, R. J., Wang, S. and Dent, S. Y. (2011). Chromatin signaling to kinetochores: transregulation of Dam1 methylation by histone H2B ubiquitination. *Cell* **146**, 709-719.
Lee, I. and Schindelin, H. (2008). Structural insights into E1-catalyzed ubiquitin activation and transfer to conjugating enzymes. *Cell* **134**, 268-278.
Liu, H. Y. and Pfleger, C. M. (2013). Mutation in E1, the ubiquitin activating enzyme, reduces Drosophila lifespan and results in motor impairment. *PLoS ONE* **8**, e32835.
Liu, D., Vleugel, M., Backer, C. B., Hori, T., Fukagawa, T., Cheeseman, I. M. and Lampson, M. A. (2010). Regulated targeting of protein phosphatase 1 to the outer kinetochore by KNL1 opposes Aurora B kinase. *J. Cell Biol.* **188**, 809-820.
Longtine, M. S., McKenzie, A., Demarini, D. J., III, Shah, N. G., Wach, A., Brachat, A., Philippsen, P. and Pringle, J. R. (1998). Additional modules for versatile and economical PCR-based gene deletion and modification in Saccharomyces cerevisiae. *Yeast* **14**, 953-961.
Lorenz, S., Cantor, A. J., Rape, M. and Kuriyan, J. (2013). Macromolecular juggling by ubiquitylation enzymes. *BMC Biol.* **11**, 65.
Lv, Z., Rickman, K. A., Yuan, L., Williams, K., Selvam, S. P., Woosley, A. N., Howe, P. H., Ogretmen, B., Smogorzewska, A. and Olsen, S. K. (2017). S. pombe Uba1-Ubc15 structure reveals a novel regulatory mechanism of ubiquitin E2 activity. *Mol. Cell* **65**, 699-714 e696.
MacKelvie, S. H., Andrews, P. D. and Stark, M. J. (1995). The Saccharomyces cerevisiae gene SDS22 encodes a potential regulator of the mitotic function of yeast type 1 protein phosphatase. *Mol. Cell. Biol.* **15**, 3777-3785.
Maerki, S., Olma, M. H., Staubli, T., Steigemann, P., Gerlich, D. W., Quadroni, M., Sumara, I. and Peter, M. (2009). The Cul3-KLHL21 E3 ubiquitin ligase targets aurora B to midzone microtubules in anaphase and is required for cytokinesis. *J. Cell Biol.* **187**, 791-800.
Makrantoni, V., Ciesiolka, A., Lawless, C., Fernius, J., Marston, A., Lydall, D. and Stark, M. J. R. (2017). A functional link between Bir1 and the saccharomyces cerevisiae Ctf19 kinetochore complex revealed through quantitative fitness analysis. *G3* **7**, 3203-3215.
Mevissen, T. E. T. and Komander, D. (2017). Mechanisms of deubiquitinase specificity and regulation. *Annu. Rev. Biochem.* **86**, 159-192.
Ng, T. M., Waples, W. G., Lavoie, B. D. and Biggins, S. (2009). Pericentromeric sister chromatid cohesion promotes kinetochore biorientation. *Mol. Biol. Cell* **20**, 3818-3827.
Nguyen, H. G., Chinnappan, D., Urano, T. and Ravid, K. (2005). Mechanism of Aurora-B degradation and its dependency on intact KEN and A-boxes: identification of an aneuploidy-promoting property. *Mol. Cell. Biol.* **25**, 4977-4992.
Nishitani, H., Goto, H., Kaneda, S., Yamao, F., Seno, T., Handley, P., Schwartz, A. L. and Nishimoto, T. (1992). tsBN75 and tsBN423, temperature-sensitive x-linked mutants of the BHK21 cell line, can be complemented by the ubiquitin-activating enzyme E1 cDNA. *Biochem. Biophys. Res. Commun.* **184**, 1015-1021.
Olsen, S. K. and Lima, C. D. (2013). Structure of a ubiquitin E1-E2 complex: insights to E1-E2 thioester transfer. *Mol. Cell* **49**, 884-896.
Pan, X., Yuan, D. S., Xiang, D., Wang, X., Sookhai-Mahadeo, S., Bader, J. S., Hieter, P., Spencer, F. and Boeke, J. D. (2004). A robust toolkit for functional profiling of the yeast genome. *Mol. Cell* **16**, 487-496.
Pedelini, L., Marquina, M., Arino, J., Casamayor, A., Sanz, L., Bollen, M., Sanz, P. and Garcia-Gimeno, M. A. (2007). YPI1 and SDS22 proteins regulate the nuclear localization and function of yeast type 1 phosphatase Glc7. *J. Biol. Chem.* **282**, 3282-3292.
Peggie, M. W., MacKelvie, S. H., Bloecher, A., Knatko, E. V., Tatchell, K. and Stark, M. J. (2002). Essential functions of Sds22p in chromosome stability and nuclear localization of PP1. *J. Cell Sci.* **115**, 195-206.
Petroski, M. D. and Deshaies, R. J. (2005). Function and regulation of cullin-RING ubiquitin ligases. *Nat. Rev. Mol. Cell Biol.* **6**, 9-20.
Pinsky, B. A., Kotwaliwale, C. V., Tatsutani, S. Y., Breed, C. A. and Biggins, S. (2006a). Glc7/protein phosphatase 1 regulatory subunits can oppose the Ipl1/aurora protein kinase by redistributing Glc7. *Mol. Cell. Biol.* **26**, 2648-2660.
Pinsky, B. A., Kung, C., Shokat, K. M. and Biggins, S. (2006b). The Ipl1-Aurora protein kinase activates the spindle checkpoint by creating unattached kinetochores. *Nat. Cell Biol.* **8**, 78-83.
Pinsky, B. A., Nelson, C. R. and Biggins, S. (2009). Protein phosphatase 1 regulates exit from the spindle checkpoint in budding yeast. *Curr. Biol.* **19**, 1182-1187.
Posch, M., Khoudoli, G. A., Swift, S., King, E. M., Deluca, J. G. and Swedlow, J. R. (2010). Sds22 regulates aurora B activity and microtubule-kinetochore interactions at mitosis. *J. Cell Biol.* **191**, 61-74.
Ramadan, K., Bruderer, R., Spiga, F. M., Popp, O., Baur, T., Gotta, M. and Meyer, H. H. (2007). Cdc48/p97 promotes reformation of the nucleus by extracting the kinase Aurora B from chromatin. *Nature* **450**, 1258-1262.
Rape, M. (2018). Ubiquitylation at the crossroads of development and disease. *Nat. Rev. Mol. Cell Biol.* **19**, 59-70.
Rizk, R. S., Discipio, K. A., Proudfoot, K. G. and Gupta, M. L. Jr. (2014). The kinesin-8 Kip3 scales anaphase spindle length by suppression of midzone microtubule polymerization. *J. Cell Biol.* **204**, 965-975.
Robinson, L. C., Phillips, J., Brou, L., Boswell, E. P. and Tatchell, K. (2012). Suppressors of ipl1-2 in components of a Glc7 phosphatase complex, Cdc48 AAA ATPase, TORC1, and the kinetochore. *G3* **2**, 1687-1701.
Rodrigo-Brenni, M. C. and Morgan, D. O. (2007). Sequential E2s drive polyubiquitin chain assembly on APC targets. *Cell* **130**, 127-139.
Rose, M. D., Winston, F. and Hieter, P. (1990). *Methods in Yeast Genetics. A Laboratory Course Manual*. Plainview, NY: Cold Spring Harbor Laboratory Press.
Ryser, S., Dizin, E., Jefford, C. E., Delaval, B., Gagos, S., Christodoulidou, A., Krause, K. H., Birnbaum, D. and Irminger-Finger, I. (2009). Distinct roles of BARD1 isoforms in mitosis: full-length BARD1 mediates Aurora B degradation, cancer-associated BARD1beta scaffolds Aurora B and BRCA2. *Cancer Res.* **69**, 1125-1134.
Salvat, C., Acquaviva, C., Scheffner, M., Robbins, I., Piechaczyk, M. and Jariel-Encontre, I. (2000). Molecular characterization of the thermosensitive E1 ubiquitin-activating enzyme cell mutant A31N-ts20. Requirements upon different levels of E1 for the ubiquitination/degradation of the various protein substrates in vivo. *Eur. J. Biochem.* **267**, 3712-3722.
Sambrook, J., E. Fritsch, and T. and Maniatis, (1989). *Molecular cloning: a laboratory manual+ cold Spring Harbor*. New York: Cold spring harbor laboratory press.
Seino, H., Kishi, T., Nishitani, H. and Yamao, F. (2003). Two ubiquitin-conjugating enzymes, UbcP1/Ubc4 and UbcP4/Ubc11, have distinct functions for ubiquitination of mitotic cyclin. *Mol. Cell. Biol.* **23**, 3497-3505.
Sherman, F., Fink, G. R. and Hicks, J. B. (1986). *Methods in Yeast Genetics*. Cold Spring Harbor NY: Cold Spring Harbor Laboratory Press.
Starita, L. M., Lo, R. S., Eng, J. K., von Haller, P. D. and Fields, S. (2012). Sites of ubiquitin attachment in Saccharomyces cerevisiae. *Proteomics* **12**, 236-240.
Straight, A. F., Marshall, W. F., Sedat, J. W. and Murray, A. W. (1997). Mitosis in living budding yeast: anaphase A but no metaphase plate. *Science* **277**, 574-578.
Straight, A. F., Sedat, J. W. and Murray, A. W. (1998). Time-lapse microscopy reveals unique roles for kinesins during anaphase in budding yeast. *J. Cell Biol.* **143**, 687-694.
Stuart, J. S., Frederick, D. L., Varner, C. M. and Tatchell, K. (1994). The mutant type 1 protein phosphatase encoded by glc7-1 from Saccharomyces cerevisiae fails to interact productively with the GAC1-encoded regulatory subunit. *Mol. Cell. Biol.* **14**, 896-905.
Sugaya, K., Ishihara, Y., Inoue, S. and Tsuji, H. (2014). Characterization of ubiquitin-activating enzyme Uba1 in the nucleus by its mammalian temperature-sensitive mutant. *PLoS ONE* **9**, e96666.
Sumara, I., Quadroni, M., Frei, C., Olma, M. H., Sumara, G., Ricci, R. and Peter, M. (2007). A Cul3-based E3 ligase removes Aurora B from mitotic chromosomes, regulating mitotic progression and completion of cytokinesis in human cells. *Dev. Cell* **12**, 887-900.
Swaney, D. L., Beltrao, P., Starita, L., Guo, A., Rush, J., Fields, S., Krogan, N. J. and Villen, J. (2013). Global analysis of phosphorylation and ubiquitylation cross-talk in protein degradation. *Nat. Methods* **10**, 676-682.
Tanaka, T. U., Stark, M. J. and Tanaka, K. (2005). Kinetochore capture and bi-orientation on the mitotic spindle. *Nat. Rev. Mol. Cell Biol.* **6**, 929-942.
Tatchell, K., Makrantoni, V., Stark, M. J. and Robinson, L. C. (2011). Temperature-sensitive ipl1-2/Aurora B mutation is suppressed by mutations in TOR complex 1 via the Glc7/PP1 phosphatase. *Proc. Natl. Acad. Sci. USA* **108**, 3994-3999.
Tung, H. Y., Wang, W. and Chan, C. S. (1995). Regulation of chromosome segregation by Glc8p, a structural homolog of mammalian inhibitor 2 that functions as both an activator and an inhibitor of yeast protein phosphatase 1. *Mol. Cell. Biol.* **15**, 6064-6074.
Turco, E., Gallego, L. D., Schneider, M. and Kohler, A. (2015). Monoubiquitination of histone H2B is intrinsic to the Bre1 RING domain-Rad6 interaction and augmented by a second Rad6-binding site on Bre1. *J. Biol. Chem.* **290**, 5298-5310.
Vanoosthuyse, V. and Hardwick, K. G. (2009). A novel protein phosphatase 1-dependent spindle checkpoint silencing mechanism. *Curr. Biol.* **19**, 1176-1181.
Varshavsky, A. (1996). The N-end rule: functions, mysteries, uses. *Proc. Natl. Acad. Sci. USA* **93**, 12142-12149.

Varshavsky, A. (2005). Regulated protein degradation. *Trends Biochem. Sci.* **30**, 283-286.
Virshup, D. M. and Shenolikar, S. (2009). From promiscuity to precision: protein phosphatases get a makeover. *Mol. Cell* **33**, 537-545.
Vong, Q. P., Cao, K., Li, H. Y., Iglesias, P. A. and Zheng, Y. (2005). Chromosome alignment and segregation regulated by ubiquitination of survivin. *Science* **310**, 1499-1504.
Wagner, S. A., Beli, P., Weinert, B. T., Nielsen, M. L., Cox, J., Mann, M. and Choudhary, C. (2011). A proteome-wide, quantitative survey of in vivo ubiquitylation sites reveals widespread regulatory roles. *Mol. Cell. Proteomics* **10**, M111 013284.
Weinert, T. A. and Hartwell, L. H. (1988). The RAD9 gene controls the cell cycle response to DNA damage in Saccharomyces cerevisiae. *Science* **241**, 317-322.
Weinert, T. A. and Hartwell, L. H. (1990). Characterization of RAD9 of Saccharomyces cerevisiae and evidence that its function acts posttranslationally in cell cycle arrest after DNA damage. *Mol. Cell. Biol.* **10**, 6554-6564.
Wickliffe, K., Williamson, A., Jin, L. and Rape, M. (2009). The multiple layers of ubiquitin-dependent cell cycle control. *Chem. Rev.* **109**, 1537-1548.
Wilson, I. A., Niman, H. L., Houghten, R. A., Cherenson, A. R., Connolly, M. L. and Lerner, R. A. (1984). The structure of an antigenic determinant in a protein. *Cell* **37**, 767-778.
Winzeler, E. A., Shoemaker, D. D., Astromoff, A., Liang, H., Anderson, K., Andre, B., Bangham, R., Benito, R., Boeke, J. D., Bussey, H. et al. (1999). Functional characterization of the S. cerevisiae genome by gene deletion and parallel analysis. *Science* **285**, 901-906.
Wood, A., Krogan, N. J., Dover, J., Schneider, J., Heidt, J., Boateng, M. A., Dean, K., Golshani, A., Zhang, Y., Greenblatt, J. F. et al. (2003). Bre1, an E3 ubiquitin ligase required for recruitment and substrate selection of Rad6 at a promoter. *Mol. Cell* **11**, 267-274.
Wurzenberger, C., Held, M., Lampson, M. A., Poser, I., Hyman, A. A. and Gerlich, D. W. (2012). Sds22 and Repo-Man stabilize chromosome segregation by counteracting Aurora B on anaphase kinetochores. *J. Cell Biol.* **198**, 173-183.
Yamagishi, Y., Honda, T., Tanno, Y. and Watanabe, Y. (2010). Two histone marks establish the inner centromere and chromosome bi-orientation. *Science* **330**, 239-243.
Ye, Y., Meyer, H. H. and Rapoport, T. A. (2003). Function of the p97-Ufd1-Npl4 complex in retrotranslocation from the ER to the cytosol: dual recognition of nonubiquitinated polypeptide segments and polyubiquitin chains. *J. Cell Biol.* **162**, 71-84.
Zhang, S., Guha, S. and Volkert, F. C. (1995). The *Saccharomyces SHP1* gene, which encodes a regulator of phosphoprotein phosphatase 1 with differential effects on glycogen metabolism, meiotic differentiation, and mitotic cell cycle progression. *Mol. Cell. Biol.* **15**, 2037-2050.
Zhang, K., Lin, W., Latham, J. A., Riefler, G. M., Schumacher, J. M., Chan, C., Tatchell, K., Hawke, D. H., Kobayashi, R. and Dent, S. Y. (2005). The set 1 methyltransferase opposes ipl 1 aurora kinase functions in chromosome segregation. *Cell* **122**, 723-734.